CRISPR-mediated activation of biosynthetic gene clusters for bioactive molecule discovery in filamentous fungi

Indra Roux[1], Clara Woodcraft[1], Jinyu Hu[1], Rebecca Wolters[1], Cameron L.M. Gilchrist[1], Yit-Heng Chooi[1]

[1]School of Molecular Sciences, University of Western Australia, Perth, WA 6009, Australia.

Correspondence to: yitheng.chooi@uwa.edu.au

Abstract

Accessing the full biosynthetic potential encoded in the genomes of fungi is limited by the low expression of many biosynthetic gene clusters (BGCs) under standard culture conditions. In this work, we develop a fungal CRISPR activation (CRISPRa) system for targeted upregulation of biosynthetic genes, which could accelerate the emerging genomics-driven approach to bioactive secondary metabolite discovery. We construct a fungal CRISPR/dLbCas12a-VPR system and demonstrate activation of a fluorescent reporter in *Aspergillus nidulans*. Then, we target the native nonribosomal peptide synthetase-like (NRPS-like) gene *micA* in both chromosomal and episomal contexts, achieving increases in production of the compound microperfuranone. Finally, multi-gene CRISPRa leads to the discovery of the *mic* cluster product as dehydromicroperfuranone. Additionally, we demonstrate the utility of the variant LbCas12a^{D156R}-VPR for CRISPRa at lower culture temperatures. This is the first demonstration of CRISPRa in filamentous fungi, providing a framework for CRISPR-mediated transcriptional activation of fungal BGCs.

Introduction

Fungal genome mining has emerged as a promising strategy for the discovery of novel bioactive secondary metabolites (SMs)[1,2] . Genomic surveys have revealed that fungal species typically harbour 30–100 biosynthetic gene clusters (BGCs) each encoding the biosynthetic pathway required to produce a SM(s)[3]. However, the vast majority of BGCs remain uncharacterised or 'cryptic' as the products they encode are undetectable under standard culture conditions, often because BGCs remain 'silent' or lowly expressed due to tight regulatory control[1,4]. Filamentous fungi, which have yielded a plethora of SMs with pharmaceutical and agricultural applications[5], thus serve as attractive targets for genome mining of novel molecules.

Improved understanding of SM biosynthesis has led to the development of various bioinformatic tools and strategies for the prioritisation of BGCs for genome mining, increasing the chance of discovery of novel molecules or molecules with desired bioactivities[6,7]. Current

34 strategies for activating specific BGCs typically involve promoter exchange of all individual
35 genes in the BGC with strong promoters[8]. If a BGC contains a transcription factor (TF) gene,
36 overexpression via promoter exchange can activate expression of the entire BGC[9]. However,
37 in many cases this strategy requires further TF engineering[10], or cluster-specific TFs are not
38 identifiable. BGC from fungi that are genetically intractable require expression in a
39 heterologous host[5]. Filamentous fungi are the most compatible heterologous hosts for
40 expression of fungal BGCs, not requiring intron removal or codon optimization[11]. For example,
41 *Aspergillus nidulans* has been successfully utilised as a heterologous host by several groups
42 [12–14], including ours[15,16]. Whether in the native fungus or in a heterologous host, promoter
43 exchange can be cumbersome due to the need for marker recycling[13] for chromosomal
44 manipulations, or the challenging episomal cloning of multiple and often large biosynthetic
45 genes[15].

46 To access cryptic SMs more efficiently and improve the viability of pathway-specific genome
47 mining as an approach for drug discovery, new tools for programmable biosynthetic gene
48 expression are necessary. Inspired by pathway-specific TFs, we aimed to develop a CRISPR
49 activation (CRISPRa)-mediated approach for BGC activation in filamentous fungi (Fig. 1a). In
50 CRISPRa systems, DNase-deactivated RNA-guided CRISPR/dCas ribonucleoprotein
51 complexes linked to activation effectors are targeted to gene regulatory regions to increase
52 gene expression [17–19]. Taking advantage of the streamlined CRISPR RNA (crRNA) cloning
53 and multiplexing capabilities, CRISPRa of BGCs has the potential to greatly accelerate fungal
54 genome mining. CRISPRa has already been used to tune the expression of biosynthetic
55 pathways[20,21], including in ascomycetous yeasts [22,23]. However, to our knowledge, CRISPRa
56 has not yet been demonstrated in filamentous fungi.

57 In this work, we develop a suite of fungal CRISPRa vectors based on both dLbCas12a from
58 *Lachnospiraceae bacterium* Cas12a (previously known as Cpf1)[19], and dSpCas9 from
59 *Streptococcus pyogenes* fused to the tripartite VPR activator[18], and test them in *A. nidulans*.
60 We further explore the application of our CRISPR/dLbCas12a-VPR system for fungal BGC
61 activation as a tool to fuel bioactive molecule discovery.

62 Results

63 Construction and testing of fungal CRISPRa systems

64 To develop a CRISPRa system for filamentous fungi, we constructed and tested
65 CRISPR/dLbCas12a-VPR- and CRISPR/dSpCas9-VPR-based systems in the model
66 organism and chassis *A. nidulans.* To evaluate alternative strategies for expressing either

dCas effector, we created parent strains with a chromosomally integrated *dCas-VPR* expression cassette and compared their performance with entirely AMA1-episomally encoded systems. The AMA1 sequence acts as an extrachromosomal vector replicator and confers increased transformation frequency in several filamentous fungi species[24]. AMA1-bearing vectors are found at multiple copies per nucleus although their genetic stability has been reported to be limited under non-selective conditions. We built on the triple auxotrophic mutant *A. nidulans* LO8030 [25], which can maintain AMA1 vectors by complementation with the selectable markers *pyrG*, *riboB*, *pyroA*[15]. The modular nature of the AMA1 vector set allowed rapid building, testing and exchange of the different CRISPRa components. For an initial proof-of-concept, we built as test target a fluorescent reporter fusing *mCherry* to *Parastagonospora nodorum elcA* promoter (P_{elcA}), which belongs to a 'silent' polyketide synthase gene[26], and delivered it encoded on a AMA1 vector.

Cas12a systems have the potential to simplify multiplexing due to their short crRNA and their capability to process the precursor crRNA array[27]. Furthermore, crRNAs can be excised from RNA polymerase II (RNAPII)-driven transcripts[28] allowing us to build a crRNA expression cassette with *gpdA* promoter (P_{gpdA}) and *trpC* terminator (T_{trpC}) (Supplementary note 1), which are parts widely portable across fungal species[29]. We tested the CRISPRa system targeting P_{elcA} with a four-crRNA array encoded on an AMA1-pyroA vector. Due to the lack of characterization of the transcription start site (TSS) of the *elcA* gene, we targeted the crRNAs to a window 88–327bp upstream of the open reading frame start codon (Fig. 1b). After growing mycelial mass, we observed activation of *mCherry* expression in the CRISPRa transformants (Fig. 1b, Supplementary Fig. 1) compared to the no crRNA control, in both chromosomally and episomally expressed dLbCas12a-VPR systems (Fig. 1b). The results demonstrated the viability of the RNAPII-promoter P_{gpdA} to deliver LbCas12a crRNA arrays.

In parallel, we built and tested a dSpCas9-VPR system, with a sgRNA expression cassette driven by the RNA polymerase III promoter U3 from *Aspergillus fumigatus* (AfP_{U3})[30] (Supplementary note 1). In this case, four sgRNA were tested individually, targeting a window 162–342 bp from the reporter start codon, and delivered in a single AMA1-pyrG vector together with the reporter construct P_{elcA}-*mCherry*. We observed that the system with chromosomal expression of *dSpCas9-VPR* resulted in activation levels only noticeable at prolonged exposure times, while the system with episomally expressed dSpCas9-VPR resulted in stronger fluorescence (Fig. 1c, Supplementary Fig. 2a and b). A possible interpretation is that the single-copy chromosomal *dSpCas9-VPR* cassette failed to achieve expression levels above the required threshold for strong observable activity, making the multicopy AMA1-encoded system more effective in comparison. We also observed a sgRNA-dependent variation in the activation intensity (Supplementary Fig. 2b). We further attempted

to deliver sgRNAs from an independent AMA1-pyroA vector, but when co-transformed with the reporter vector and the dSpCas9-VPR expression vector, fluorescence was not observed (Supplementary Fig. 2c).

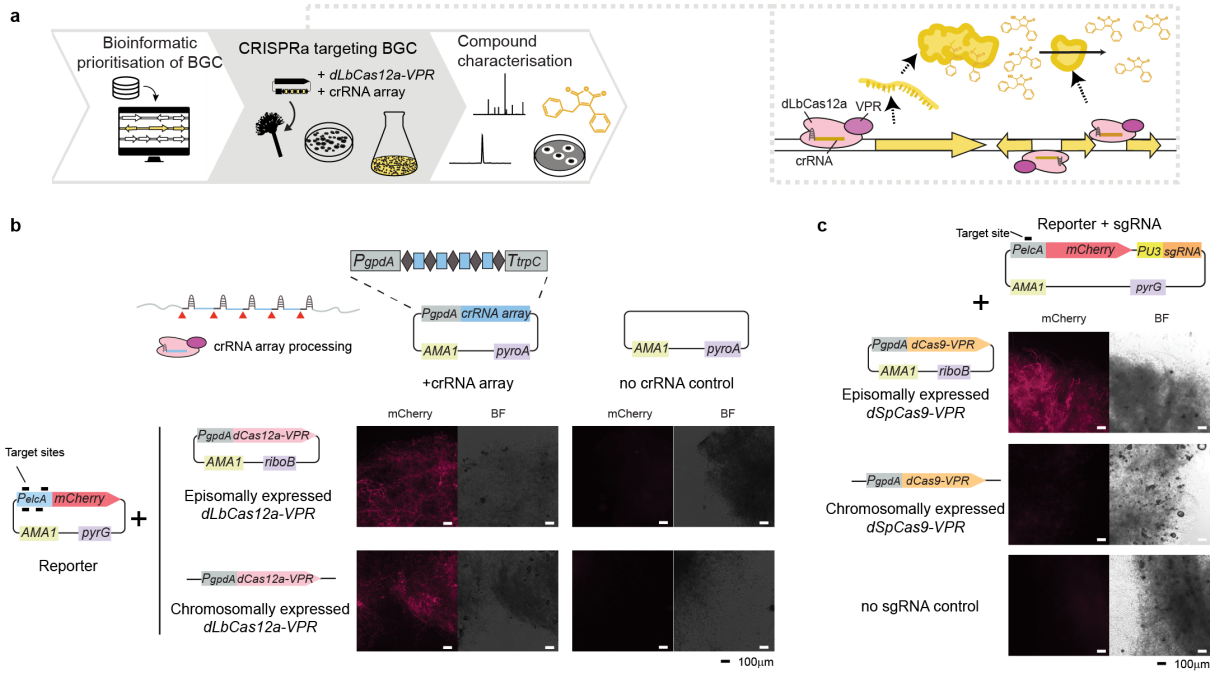

Fig. 1 Proof-of-concept for fungal CRISPRa **a.** Schematic of a CRISPRa-based genome mining pipeline. After BGC bioinformatic prioritisation, the designed crRNAs are rapidly assembled in an expression vector and transformed into the fungal host along with the dCas effector. The CRISPRa complex is targeted to the regulatory regions of the selected BGC, upregulating gene expression and consequently increasing production of the encoded compound(s). This would facilitate compound detection, screening for bioactivity and further chemical characterisation. **b.** CRISPR/dCas12a-VPR mediated activation of P_{elcA}-*mCherry* in *A. nidulans.* Representative fluorescent microscopy images of CRISPRa transformant mycelia demonstrate consistent *mCherry* reporter activation, which implies the processing of crRNA array from a P_{gpdA}-derived RNAPII-driven transcript by dLbCas12a-VPR. Activation is observed both episomally and chromosomally encoded dLbCas12a-VPR systems (Supplementary Fig. 1). **c.** Activation strength of the CRISPR/dSpCas9-VPR system showed dependency on dSpCas9-VPR expression strategy (Supplementary Fig. 2). In all microscopy images mycelia were observed under brightfield (BF) and mCherry filter after overnight growth on stationary liquid culture at 37 °C. Scale bar 100 μm.

Activating *micA* for increased microperfuranone production

As CRISPR/dLbCas12a-VPR demonstrated better versatility in our initial tests, we decided to proceed to the next phase with this system. To test whether CRISPR/dLbCas12a-VPR mediated activation of fungal biosynthetic genes could induce metabolite production, we targeted the native *A. nidulans micA* (*AN3396*) gene which encodes a nonribosomal peptide synthetase-like (NRPS-like) enzyme responsible for the biosynthesis of microperfuranone (**1**) (Fig. 2a). The biosynthetic function of *micA* had been previously decoded by Yeh et al.[31],

129 following a promoter replacement strategy, after unsuccessful attempts to elicit the
130 biosynthesis of cryptic NRPS-like products by varying *A. nidulans* culture conditions.

131 Based on available *A. nidulans* TSS annotation[32,33], we followed previously devised guidelines
132 for CRISPRa in eukaryotes[34] and targeted a region 119–303 bp upstream of the TSS with a
133 four-crRNA array named MU (*micA* Upstream TSS) (Fig. 2b). To explore the utility of CRISPRa
134 for genes that lack TSS information, which is the case for 59% of *A. nidulans* BGC genes
135 (Supplementary Fig. 3a), we also tested an alternative TSS annotation-blind targeting criteria,
136 taking the gene start codon as reference. Given that most *A. nidulans* BGC genes have short
137 5′ untranslated region (UTR) (Supplementary Fig. 3b), we targeted a window 139–324 bp
138 upstream of the *micA* start codon with a four-crRNA named MD (*micA* Downstream TSS),
139 which in this case corresponds to the 5′ UTR of *micA.* Analysis by liquid chromatography
140 coupled to a diode array detector and mass spectrometer (LC-DAD-MS) showed increases in
141 the production of **1** in media extracts from all CRISPRa transformants when compared to the
142 background levels in the controls (Fig. 2c). Interestingly, targeting the 5′ UTR of *micA* with
143 crRNA array MD resulted in significantly higher production than when targeting the *micA*
144 promoter region with crRNA array MU, with titres of **1** up to 0.6 mg L^{-1} (Fig. 2d).
145 Nevertheless, targeting with MU still led to a ~4.5-fold increase in production with a titre up to
146 0.2 mg L^{-1} compared to the controls. No significant difference in performance was observed
147 when comparing between chromosomally and episomally expressed dLbCas12a-VPR
148 systems for both crRNA arrays.

149 In order to enable rapid cloning of different crRNAs for further testing, we established a
150 domesticated version of the AMA1-pyroA expression vector, which allowed one-step Type IIS
151 cloning of crRNA arrays using annealed oligonucleotides (Supplementary Fig. 4). We verified
152 the null effect of P_{gpdA} promoter domestication (Supplementary Fig. 4b).

153 To examine the effect of each crRNA in *micA* activation, individual crRNAs from MD and MU
154 arrays were delivered in strains harbouring chromosomally integrated *dLbCas12a-VPR* (Fig.
155 2e and Supplementary Fig. 5). We observed a minimal increase in the production of **1** when
156 targeting with some MD crRNA, while in most cases the production of **1** was indistinguishable
157 from the no crRNA control. The broad difference between the production of **1** in strains with
158 single crRNAs and the observed with multiple-crRNA array CRISPRa is indicative of a
159 synergistic activation effect (Fig. 2e).

160 To test whether the production of **1** could be further increased, we targeted *micA* with both
161 MD and MU crRNA arrays simultaneously. To this end, we re-cloned the crRNA array MD into
162 an AMA1-pyrG vector to allow co-transformation with the crRNA array MU encoded on an
163 AMA1-pyroA vector. Co-transformation of both MD and MU crRNA arrays for *micA* activation

resulted in further increase in the production of **1** (up to ~0.8 mg L^{-1}) (Supplementary Fig. 6). Interestingly, the crRNA array MD alone delivered from the AMA1-pyrG vector resulted in a considerable increase in the titre of **1** compared to when delivered using AMA1-pyroA vector, which might contribute to the dual crRNA array increased production (Supplementary Fig. 6).

Finally, to evaluate the broader utility of CRISPRa targeting episomal genes in *A. nidulans*, we co-transformed additional copies of *micA* encoded on an AMA1 vector. The transformants harbouring episomal copies of *micA* with its full-length promoter showed relatively high basal production of **1** even in the absence of CRISPRa (Fig. 2f). However, we still observed a consistent increase in the titres of **1** when CRISPRa of *micA* was performed with either MD or MU crRNA arrays, reaching up to over 4 mg L^{-1} (Fig. 2f). We further tested targeting a shorter episomal *micA* variant with low basal production of **1**. When co-transforming with MD, targeting the still-present 5′ UTR, we observed the largest activation fold change with a ~30-fold increase in the production of **1** compared to the control, reaching final titres of ~1.5 mg L^{-1} (Fig. 2g). Taken together, these results show that CRISPRa can affect the expression of episomally encoded genes, as the increase in the production of **1** is not explained by the activation of chromosomal *micA* alone.

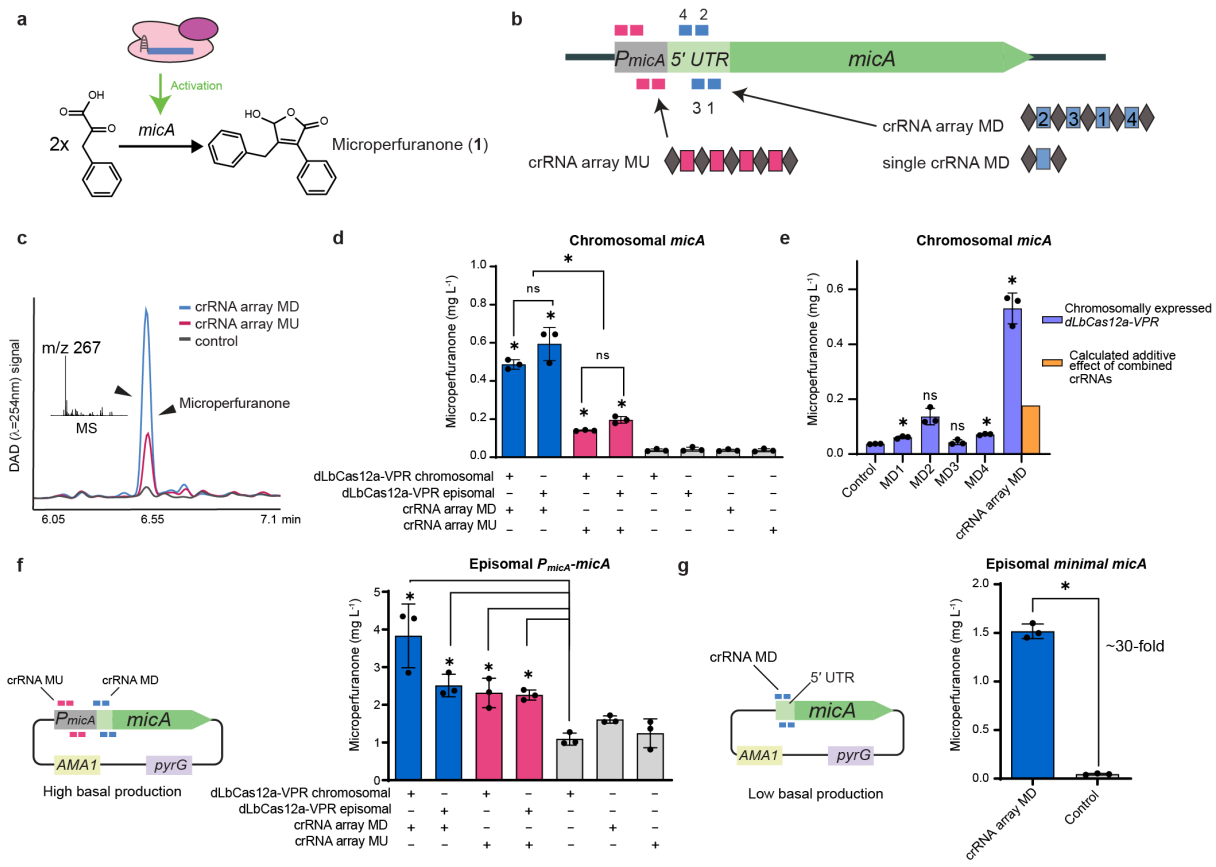

Fig. 2 . CRISPRa-mediated microperfuranone (**1**) production. **a.** Upregulation of *micA* results in the biosynthesis of **1** from two phenylpyruvate[31]. **b.** Chromosomal *micA* gene with individual crRNA binding sites shown in magenta (crRNA array MU) and blue (crRNA array MD).

Numbers assigned to MD crRNAs are indicative of targeting position in respect to *micA* start codon, with their position in the crRNA array MD also indicated in the scheme. **c.** DAD (λ=254 nm) chromatograms of *A. nidulans* culture media extracts show increases in the peak identified as **1** in strains with CRISPR-mediated activation of *micA* (magenta and blue) as compared to the control with no crRNA (grey). Expected mass of **1** is observed as main ion in the peak by MS. **d.** CRISPR-mediated activation of chromosomal *micA*. All CRISPRa strains showed a significant increase in the production of **1** compared to their respective dLbCas12a-VPR control with no crRNA. Targeting CRISPRa with MD crRNA array (blue) resulted in significantly higher production of **1** compared to targeting with MU crRNA (magenta). There was no significant difference between both dLbCas12a-VPR expression strategies. **e.** When targeting *micA* with single MD crRNAs low or no activation is observed compared to the no crRNA control. The low calculated additive of single crRNA CRISPRa (described in Methods) suggests a synergistic activation effect when making use of the four-crRNA array MD. **f.** Increases in the titre of **1** are observed in media extracts of CRISPRa strains with extra episomal *micA* copies (high basal production) compared to the no crRNA control in strains with episomal *micA* vector. **g.** In strains harbouring episomal copies of a shorter *micA* variant (low basal production), CRISPRa increased the production of **1** by ~30-fold compared to the control. In all the figures, calculated titre (mg L^{-1}) values are the mean of three biological replicates which specific values are indicated as black dots, error bars represent SD. Two-sided Welch's T-test with Holm-Šídák multiplicity correction per figure was performed. Asterisk indicates corrected P-value<0.05, (ns) not significant. Individual P-values are listed in Supplementary Table 9.

Multi-gene activation uncovered cryptic gene cluster product

The gene *micA* (*AN3396*) has been proposed to belong to a BGC, which also contains a putative cytochrome P450 (*AN3394*) and an hypothetical gene (*AN3395*)[31,35], henceforth referred to as *micB* and *micC*, respectively. However, the final product of the *mic* cluster has remained uncharacterised.

To assess the feasibility of performing simultaneous activation of multiple genes with CRISPR/dLbCas12a-VPR, we aimed to co-activate the proposed *mic* cluster. We co-transformed the four-crRNA array MD targeting *micA* along with a second crRNA array targeting *micB* and *micC* (Fig. 3a). This new three-crRNA array, named crRNA array P, targeted a window of 209bp in the middle of the short 396 bp bi-directional promoter between the divergently oriented *micB* and *micC* genes. We delivered the two crRNA arrays from independent AMA1 episomal vectors in strains harbouring chromosomally integrated *dLbCas12a-VPR* (Fig. 3a). To account for the above-mentioned influence of the crRNA delivery vector selection marker on CRISPRa strength, we tested both dual plasmid delivery combinations with *pyrG* and *pyroA* selection markers (Fig. 3a).

LC-DAD-MS analysis of *A. nidulans* culture extracts showed that both multiplexed-CRISPRa strains presented a decrease in the precursor microperfuranone (**1**) and an increase in the production of three new peaks detected by DAD and MS, arbitrarily named peaks I, II and III (Fig. 3c, Supplementary Fig. 7a–b). However, the magnitude of the changes in the metabolic

225 profile was dependent on the marker combination used in the delivery of the crRNA arrays.
226 Given that the precursor **1** does not appear to be limiting as it remains present under all
227 configurations, crRNA array P delivery on an AMA1-pyrG vector favoured the production of
228 the peaks I–III compared to when delivered on AMA1-pyroA (Fig. 3d). We further tested the
229 best performer crRNA array delivery combination switching to episomally encoded
230 *dLbCas12a-VPR* and observed an increased production of the peaks I–III relative to the peak
231 from **1** (Fig. 3d, Supplementary Fig. 7c). Taken together these results indicate that multiple
232 gene CRISPRa can be used to explore the metabolite products of a cryptic BGC and that the
233 activity can be tuned to favour the final product of the cluster.

234 The observed mass of the ions accumulated in the peaks I-III was m/z 265 $[M+H]^+$, 2 Da less
235 than the molecular mass of **1**, suggesting that an oxidation has occurred. Searching the
236 chemical literature for structures related to **1** corresponding to a mass of 264 Da led us to a
237 previously reported metabolite, 3-carboxy-2,4-diphenyl-but-2-enoic anhydride, herein
238 renamed as dehydromicroperfuranone (**2**) (Fig. 3b) first isolated from *A. nidulans* IFO 6398 as
239 a plant growth promoting compound[36]. We further analysed the CRISPRa strain crude extract
240 by LC-MS/MS and observed that the fragmentation pattern of the 265 m/z ions shared almost
241 all masses with the predicted spectra for **2** by CFM-ID[37] (Supplementary Table 1).

242 To ensure that the production of the peaks I–III is due to CRISPRa co-targeting the *micB–C*
243 promoter, we further verified the final product of the *mic* cluster by promoter replacement of
244 *micA*, *micB* and *micC*. When expressing *micA* and *micB* from alcohol inducible promoters, the
245 metabolic profile presented the peaks I–III as observed by CRISPRa, although the metabolites
246 were produced in higher quantities (Supplementary Fig. 8a). The co-expression of *micA–C*
247 resulted in the same metabolic profile as *micA–B* (Supplementary Fig. 8a). This revealed the
248 function of MicB as a cytochrome P450 monooxygenase responsible for converting a
249 secondary alcohol on **1** to a ketone group, forming a maleic acid anhydride moiety.

250 To corroborate the structure of the compounds, we attempted to purify the peaks I–III. The
251 peaks I-II co-eluted during semi-preparative HPLC purification, while peak III could be isolated
252 as a single peak. Surprisingly, the ^{1}H-NMR and ^{13}C-NMR spectra of the peaks I-II mixture and
253 peak III in deuterated chloroform appear to be identical (Supplementary Table 2 and
254 Supplementary Fig. 9–12), and both matched the previously reported chemical shifts for **2** [36].
255 When reconstituting the NMR sample in methanol for analysis by LC-DAD-MS, the purified
256 peaks reverted to multiple peaks (Supplementary Fig. 8c) and we further observed that the
257 samples also exist as mixtures when analysed by NMR in deuterated methanol
258 (Supplementary Fig. 13–14). These results suggest that the compounds in the peaks I-III are
259 interchangeable tautomeric or opened/closed ring forms in acetonitrile or methanol

260 (Supplementary Fig. 8d) but existed as a single entity in chloroform during NMR analysis
261 (Supplementary Table 2). Taken together, the results from LC-MS/MS and NMR analysis
262 supported that the metabolite product of the *mic* cluster as **2**.

263 Due to increased polarity, **2** was only extractable from the culture medium with acidified ethyl
264 acetate or adsorbent resin (Supplementary Fig. 8b) , which might explain why this compound
265 has not been observed in previous studies where ethyl acetate extraction was used for
266 metabolite profiling of *A. nidulans*[31,38] .

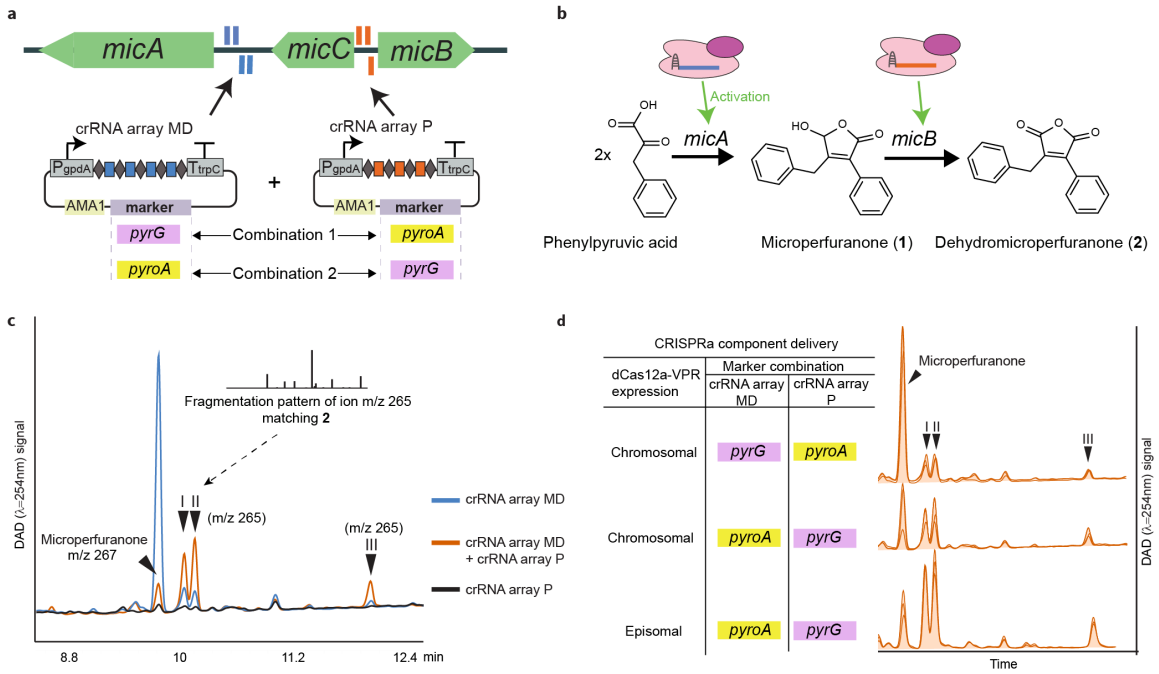

267

268 **Fig. 3.** Elucidating the *mic* cluster final product with multi-gene activation **a.** Schematic of the
269 experimental set-up of *mic* cluster activation with two-vector crRNA arrays delivery and
270 different markers combinations of *pyrG* (purple) and *pyroA* (yellow). The *mic* cluster genes are
271 shown in green alongside the target sites of crRNA MD array (blue) and crRNA P array
272 (orange). **b.** Proposed dehydromicroperfuranone (**2**) structure and biosynthetic pathway. **c.**
273 Representative overlaid DAD (λ=254 nm) chromatograms of media extracts from strains with
274 both crRNA arrays MD and P (orange), crRNA array MD (blue) and crRNA array P (black).
275 Multi-gene CRISPRa results in the increase of the peaks I–III whose main ion *m/z* 265 yielded
276 a fragmentation pattern matching **2** by LC-MS/MS analysis (Supplementary Table 1). **d.**
277 Production of each peak in multiple activation strains is dependent on CRISPRa component
278 delivery strategy. The different DAD (λ=254 nm) chromatograms represent three biological
279 replicates per delivery strategy (Supplementary Fig. 7). We observe that the production of the
280 peaks I–III is favoured in the marker combination crRNA MD in an AMA1-pyroA vector and
281 crRNA P in an AMA1-pyrG vector.

282 **dLbCas12a^{D156R} improves activation at lower temperatures**

283 The activity of Cas12a systems is modulated by temperature[39]. This could compromise the
284 applicability of fungal CRISPRa, as the majority of fungi have optimum growth temperatures
285 between 25 °C and 30 °C[40] and the production of some SMs is favoured at lower

286 temperatures[1]. To evaluate CRISPRa performance at lower temperatures, we observed
287 CRISPR/dSpCas9-VPR and CRISPR/dLbCas12a-VPR mediated activation of the P_{elcA}-
288 *mCherry* reporter across multiple temperatures. The fluorescence observed at 30 °C was
289 comparable to the samples grown at 37 °C in both systems, but at 25 °C only observable in
290 CRISPR/dSpCas9-VPR samples although at lower intensity (Supplementary Fig. 15).

291 Due to the restrictions on dLbCas12a-VPR activity at 25 °C a putative temperature tolerant
292 variant was investigated. Taking inspiration from the AsCas12a^{E174R} variant, recently reported
293 to possess increased double stranded DNA cleavage efficiency *in vitro* at 25 °C[41], we built an
294 LbCas12a mutant harbouring the homologous mutation D156R identified by aligning the
295 AsCas12a/LbCas12a crystal structures[42,43] (Supplementary Fig. 16).

296 We tested the variant dLbCas12a^{D156R}-VPR targeting chromosomal *micA* with the crRNA array
297 MD. We observed significant CRISPR/dLbCas12a^{D156R}-VPR mediated activation at 25 °C, a
298 temperature at which CRISPR/dLbCas12a mediated activation was not observed (Fig. 4b).
299 However, at 37 °C CRISPR/dLbCas12a^{D156R}-VPR achieved lower final production of **1** than
300 the original dLbCas12a-VPR system (Fig. 4b). We also observed evidence of
301 CRISPR/dLbCas12a^{D156R}-VPR mediated fluorescence activation at 25 °C (Fig. 4a,
302 Supplementary Fig. 15).

303 The presence of protospacer adjacent motif (PAM) near the target is a critical requirement for
304 CRISPR systems, in the case of LbCas12a systems the sequence TTTV [44]. The variant
305 LbCas12a^{D156R} has been reported to exhibit improved recognition of the non-canonical PAM
306 sequence TTCN [45]. We tested a poly-crRNA array targeting TTCN PAM sites in the 5′ UTR of
307 *micA*, and observed an improved activation mediated by the dLbCas12a^{D156R} variant over the
308 original dLbCas12a system at 37 °C (Fig. 4b). In most *A. nidulans* BGC genes around 10
309 canonical TTTV PAM sites can be found in a targetable window for activation (Supplementary
310 Fig. 17). Nevertheless, targeting TTCN can be considered if PAM site availability is a limiting
311 factor.

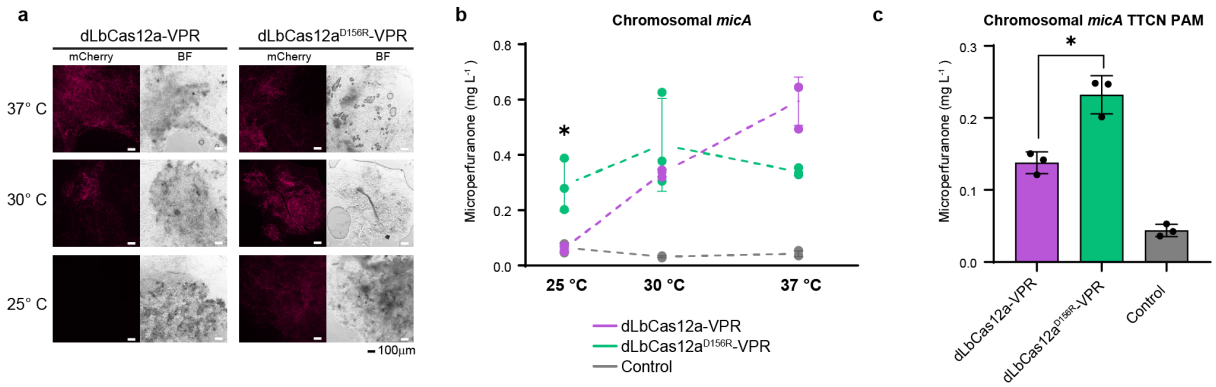

312

313 **Fig. 4.** The variant dLbCas12a^{D156R}-VPR outperforms at some limiting conditions for
314 dLbCas12a-VPR. **a.** Representative microscopy images of *A. nidulans* mycelia grown at
315 different temperatures show that CRISPR/dLbCas12a-VPR mediated activation of the
316 fluorescent reporter P_{elcA}-*mCherry* is restricted at 25 °C. The variant dLbCas12a^{D156R}-VPR
317 presents observable fluorescence at 25 °C unlike the original system (Supplementary Fig. 15).
318 In all microscopy images mycelia were observed under brightfield (BF) and mCherry filter.
319 Scale bar 100 μm. **b.** *A. nidulans* growth temperature of 25°C is limiting for
320 CRISPR/dLbCas12a-VPR mediated *micA* activation (purple), as no increments in
321 microperfuranone (**1**) are observed. The variant dLbCas12a^{D156R}-VPR (green) demonstrated
322 CRISPRa activity at 25°C, achieving a ~4.5-fold increase in the production of **1** compared to
323 the no crRNA control. However, the activity of dLbCas12a^{D156R}-VPR was limited compared to
324 the original dLbCas12a-VPR system at 37 °C**. c.** Activity at the alternative PAM site TTCN is
325 increased by the dLbCas12a^{D156R}-VPR variant. In all figures, calculated titre (mg L^{-1}) values
326 are the mean of three biological replicates whose specific values are indicated as dots, error
327 bars represent SD. Two-sided Welch's T-test with was performed. Asterisk indicates corrected
328 P-value<0.05. Individual P-values are listed in Supplementary Table 9.

329 ## Discussion

330 In this work, we reported the first application of CRISPRa in an ascomycetous filamentous
331 fungus belonging to the Pezizomycotina taxon, known to harbour diverse BGCs. We first
332 tested different strategies for expressing both CRISPR/dSpCas9-VPR and
333 CRISPR/dLbCas12a-VPR system components in *A. nidulans*, observing the activation of a
334 fluorescent reporter. We then demonstrated the feasibility of CRISPR/dLbCas12a-VPR
335 mediated activation of *A. nidulans* native biosynthetic genes to induce SM production. This led
336 to the rediscovery of dehydromicroperfuranone, in which the molecule was associated with
337 the *mic* cluster for the first time. Additionally, we demonstrated CRISPRa-mediated
338 upregulation of genes in episomal constructs, which could be a valuable tool to activate BGCs
339 from diverse fungi captured on vectors and heterologously expressed in *A. nidulans* as a
340 chassis[12,15].
341 The CRISPR/dLbCas12a-VPR system presented advantages in multiplexing capability and
342 supported expression of CRISPRa components in various configurations. Additionally, as
343 Cas12a successfully processed transcripts driven by the RNAPII promoter P_{gpdA}, it allowed us
344 to build an AMA1-derived CRISPRa vector set with common fungal genetic parts, increasing
345 the potential portability of the CRISPRa system across fungal species. We targeted *micA* with
346 multiple crRNAs to increase the likelihood of achieving strong activation, an approach used in
347 pooled CRISPRa screenings[46], and observed a synergistic activation effect. Cas12a has been
348 demonstrated to process up to 25 crRNAs from a single transcript in the literature[47] , indicating
349 that CRISPR/dCas12a systems may have the potential to extend multiplexing to target whole
350 BGCs from a single crRNA array in future works. Additionally, next generation activators[48]
351 could improve dCas12a-based CRISPRa activation strength.

352 We also explored the viability of selecting crRNA targets in a TSS annotation-blind manner,
353 considering filamentous fungi genomes in public databases often lack 5′ UTR annotations. In
354 the case of *micA*, targeting a short distance upstream of the gene start codon, despite falling
355 in the 5'UTR, resulted in successful production of microperfuranone. This is surprising, as it
356 contradicts the possible roadblock of transcription effect[22], and might imply that the binding of
357 dLbCas12a-VPRs to *micA* 5′ UTR region redefines the local transcriptional landscape by other
358 means[49]. Although this might be a locus-specific effect, exploring TSS annotation-blind criteria
359 could be a viable alternative when targeting BGCs with incomplete gene annotation, as
360 demonstrated for P_{elcA} and *micA.*
361 Considering the potential limitation of dLbCas12a-VPR in filamentous fungi with low optimal
362 growth temperatures, we built and tested dLbCas12a^{D156R}-VPR. During the preparation of this
363 manuscript, the LbCas12a^{D156R} variant was reported to exhibit increased low-temperature
364 genome editing efficiency *in vivo*[50]*.* Here, we demonstrated that the temperature tolerance
365 property is translatable to CRISPRa, allowing activity at limiting temperatures for the original
366 system.
367 In conclusion, we believe this work represents a valuable expansion to the fungal CRISPR
368 toolbox and provides a foundation for the further development of CRISPR-based
369 transcriptional activators as a tool for the discovery of novel fungal SMs. The CRISPRa vector
370 set could also contribute to SM discovery by targeting different combinations of genes and
371 aiding the elucidation of the resulting SM intermediates, interrogating BGC regulation with
372 specific epigenetic effectors as well as interrogation of other related biological functions.

373 Methods

374 Plasmids Construction

375 Main vectors for the Cas12a systems will be deposited in Addgene. All vectors are listed along
376 with their description and the cloning method used in Supplementary Table 4. Plasmids were
377 generated using one of the following methods: restriction enzyme cloning with PacI, NotI and
378 T4 DNA ligase; Type IIS assembly with BsmbI and annealed oligo cloning; yeast homologous
379 recombination or isothermal assembly with NEBuilder HiFi DNA Assembly Master Mix (NEB).
380 All primers used are listed in Supplementary Table 8 along with their destination construct and
381 source of DNA template. The AMA1 fungal vector pKW20088[51], was a gift from Prof Kenji
382 Watanabe, University of Shizuoka, and the vectors pYFAC-riboB, pYFAC-pyroA, pYFAC-
383 CH2, pYFAC-CH3,pYFAC-CH4 were built previously[15]. In all cases when amplifying P_{gpdA} and
384 T_{trpC} consisted in the sequences delimited in the expression cassette from pBARGPE1[29],
385 (obtained from the Fungal Genetics Stock Centre) or the modified version pBARGPE1-LIC[52].
386 To clone dSpCas9-VPR it was amplified from pAG414GPD-dCas9-VPR[18], which was a gift

387 from George Church (Addgene plasmid #63801). dLbCas12a^{D832A} was amplified from a
388 plasmid kindly provided by Christian Pflüger which was constructed from pY027[53], a gift from
389 Feng Zhang (Addgene plasmid # 84742) , by site-directed mutagenesis. and fused to VPR
390 amplified from pAG414GPD-dCas9-VPR[18]. P_{elcA} was amplified from pYFAC-CH6[15]. The
391 coding sequence of *mCherry* was amplified from pMP7601[54] which was a gift from Alex
392 Andrianopoulos (University of Melbourne). *A. nidulans* sequences were PCR amplified from
393 *A. nidulans* LO8030 gDNA (chromosomal coordinates indicated in Supplementary Table 5)[55].
394 AfP_{U3} was amplified from *Aspergillus fumigatus* 293 gDNA. And adapted version of pGEM-T
395 (Promega) was used to build the Step 1 crRNA and sgRNA cloning vector. The Cas9 sgRNA
396 cloning cassette was synthesised as gBlock and re amplified when fused to AfP_{U3} (Sequence
397 at Supplementary note 1). P_{gpdA} crRNA cloning cassette was created by annealed oligo cloning
398 (Sequence at Supplementary note 1). BsmbI domesticated one-step-cloning vector pCRI008
399 was built by PCR site directed mutagenesis of PYFAC-pyroA parts (Supplementary Fig. 4a).

400 **sgRNA and crRNA design and cloning**

401 The target sequences of each crRNA or sgRNA are listed in Supplementary Table 6, along
402 with the PAM sequence and relative distance to target gene start codon and TSS[55]. The
403 spacers were also verified to pass the bioinformatic off-target test against *A. nidulans* FGSCA4
404 genome sequence with EuPaGDT[56]. All crRNA and sgRNA were synthesised as
405 oligonucleotides with overhangs, as listed in Supplementary Table 7. Oligos were mixed in
406 equal proportion (10nM), annealed on a thermocycler , phosphorylated in the case of crRNA
407 arrays and ligated with T4 DNA ligase in previously BsmbI digested vectors.

408 For some Cas12a crRNA, one-step cloning was possible in the fungal crRNA expression
409 vector pCRI008. For the rest, crRNA were cloned by a 2-vector cloning procedure
410 (Supplementary Fig. 4c). In that case, oligos with encoded crRNA were first cloned into the
411 pGEM-T derived vector pCRI007, and the expression cassette further PCR amplified with
412 primers that reconstituted full P_{gpdA} and added homology arms. The amplicon was then cloned
413 to the final YFAC fungal vector with homology-based cloning.

414 For Cas9 sgRNA, the sgRNAs were first cloned into pCRI010, and the PacI NotI flanked
415 expression cassette digested, purified and ligated to a PacI NotI digested pCRI011 reporter
416 vector.

417 ***A. nidulans* strains construction and transformation**

418 *A. nidulans* strains with either dCas9-VPR and dCas12a-VPR chromosomal expression
419 cassettes were created by polyethylene glycol (PEG)-calcium-based transformation as in Lim
420 et al.[57] with a previously linearised vector containing 1kb homology regions to facilitate

421 homologous recombination in *A. nidulans 8030* stcJΔ locus. The fragment also contained the
422 *Bar* marker, and colonies were selected for resistance to glufosinate extracted from Basta as
423 in Li et al.[16] and the event confirmed by diagnostic PCR. Complete genotype of the parental
424 strains is listed in Supplementary Table 4.

425 For each transformant strain genotype of the protoplasts used and vectors transformed are
426 listed in Supplementary Table 4, along with the strategy to supplement all auxotrophies.
427 *P*rotoplasts of *A. nidulans* LO8030, dCas-VPR expressing parental strains were prepared from
428 germlings as in Lim et al.[57], mixed with a quarter volume PEG 60% to a final concentration of
429 10^8 protoplasts per ml and frozen at -80 °C for later use. AMA1-vectors were transformed into
430 *A. nidulans* protoplasts modifying Lim et al. 2012[57] in order to minimise the required
431 transformation volume. In a 2 mL microcentrifuge tube, 60 μL of thawed protoplast solution
432 was incubated with 50 μL of STC buffer and 3 μg of each plasmid contained in maximum total
433 volume of 10 μL. After 20 mins of incubation on ice 350 μL of the calcium PEG 60% mix was
434 added and mixed gently by inversion, followed by a 20 min incubation at room temperature.
435 After adding 1 mL of STC buffer the mix was spread on solid glucose minimal media (GMM)
436 stabilised with sorbitol (SMM), that were then incubated for three days at 37 °C to generate
437 transformant colonies.

438 **Fluorescence Microscopy**

439 Spores from individual colonies were grown overnight in an incubator when 37° C , unless
440 other incubation temperature specified, in small petri dishes containing liquid GMM to obtain
441 mycelia. Samples grown at 30 °C were incubated overnight, while samples at 25 °C were
442 grown for two days in order to harvest comparable mycelial growth. Fluorescence images
443 were captured on the epifluorescence inverted microscope Eclipse Ti2 (Nikon), using Plan
444 Apo λ 10x /0.45 numerical aperture (NA) objective lens (Nikon) and a Camera DS-Qi2 (Nikon)
445 controlled by NIS Elements Advanced Research (Nikon). Fluorescent microscopy was carried
446 out under a mCherry filter set (562/40 nm excitation, 593 nm dichroic beamsplitter, and 641/75
447 nm emission), using an 800 ms exposure and 9.6x analog gain unless specified otherwise.
448 Brightfield images captured at a 300 ms exposure time with 1x analog gain. Images were
449 recorded using NIS-Elements Advanced Research software package (Nikon).

450 **Culture conditions and crude extract preparation**

451 For each strain, three separate transformant colonies were picked as replicates for culture
452 analysis and re-streaked individually in a solidified GMM plate to be cultivated for three days
453 at 37 °C to produce spores. Spores were harvested from plates in 0.1% Tween 80 and counted
454 under Neubauer chamber, $2x10^8$ spores were inoculated into 250-ml flasks containing 50 ml

455 liquid GMM medium as described previously[15], additionally adding ampicillin to 50 μg mL^{-1} and
456 supplementing with riboflavin, uracil uridine, pyridoxine as indicated in Supplementary Table
457 4. Cultures were grown for 2.5 days with shaking set at 200 rpm and 37 °C, unless other
458 temperature indicated. In the case only of the samples needing P_{alcA} promoter induction,
459 cyclopentanone at a final concentration of 10 mM was added to the medium after 18 h of
460 incubation. At the end of the culture, 20 mL of media was collected in 50-mL Falcon tubes by
461 filtration with Miracloth. The metabolites were extracted from the liquid culture with 20 mL of
462 an organic solvent mixture containing ethyl acetate, methanol and acetic acid (89.5:10:0.5
463 ratio). The crude extracts were dried down *in vacuo* and re-dissolved in 0.3 mL of methanol
464 for LC-DAD-MS analysis.

465 **Metabolic profile analysis by LC-DAD-MS**

466 The analyses of the metabolite profiles were performed on an Agilent 1260 liquid
467 chromatography (LC) system coupled to a diode array detector (DAD) and an Agilent 6130
468 Quadrupole mass spectrometer (MS) with an electrospray ionisation (ESI) source. In all cases
469 3 μL of the methanol dissolved crude extract was injected. Chromatographic separation was
470 performed at 40 °C using a Kinetex C18 column (2.6 μm, 2.1 mm i.d. 3 100 mm; Phenomenex).
471 Chromatographic separation was achieved with a linear gradient of 5-95% acetonitrile-water
472 (containing 0.1% v/v formic acid) in 10 minutes followed by 95% acetonitrile for 3 minutes, with
473 a flow rate of 0.70 mL min^{-1}. For the multiple target CRISPRa experiments, the gradient was
474 extended to 20 min for better separation. The MS data were collected in the m/z range 100–
475 1000 in positive ion mode and UV observed at DAD λ=254.0±4.0 nm.

476 Peak areas were determined by peak integration of DAD λ=254 nm chromatogram using
477 Masshunter Workstation Qualitative Analysis (Agilent). To quantify microperfuranone (**1**)
478 samples were compared to a calibration curve. To this end, a standard of **1** was prepared by
479 weighing approximately 14 mg of purified **1** and diluting in methanol. This procedure was
480 repeated independently 3 times (Supplementary Fig. 18a), and a representative regression fit
481 to zero was used to quantify **1** (Supplementary Fig. 18b). The coefficient was used to
482 extrapolate the concentrations in the crude extract to the culture media concentrations.

483 For the calculated additive of single crRNA mediated production of **1** in Fig. 2e, the negative
484 control mean was added to the summation of the difference between the mean of each
485 individual crRNA production and the negative control mean, for the four crRNAs tested.

486 **LC-MS/MS analysis**

487 Selected samples were analysed by LC-MS/MS on a Thermo Scientific Fusion Orbitrap
488 coupled to a Thermo Ultimate 3000 UHPLC. The column used was an Agilent Poroshell 120

489 SB-C18 (2.1 x 30 mm, 2.7 µm) with a 20 min linear gradient of 5 – 95% acetonitrile-water
490 containing 0.1% v/v formic acid. Precursor ion data was collected for m/z 200 to 300 Da in
491 positive ion mode. Fragmentation was achieved with the higher-energy collisional dissociation
492 cell set to a collision energy of 15. Fragment identification was aided by CFM-ID[37] predictions
493 based on hypothesized structures.

494 **Compound isolation and NMR structural characterization**

495 For the microperfuranone (**1**) standard purification, 2 L of 2-days culture media from strain 52
496 (Supplementary Table 4), after induction, was extracted with a mix of ethyl acetate, methanol
497 and acetic acid (89.5:10:0.5). The crude extract was dried *in vacuo*, resuspended in methanol
498 and loaded onto a Sephadex LH-20 (GE Healthcare) column for fractionation. Fractions
499 containing the target compound were combined and further purified by semi-prep HPLC with
500 a C18 column (Grace, 5 µm, 10 × 250 mm) (isocratic, 40% acetonitrile-water, 4.3mL min^{-1}).

501 For purification of dehydromicroperfuranone (**2**) peaks 4 L of 2-days culture media from strain
502 54 (Supplementary Table 4), after induction, was loaded onto a customized Diaion HP-20
503 (Sigma) column pre-equilibrated with water. The column was then flushed with 2 column-
504 volume of water and eluted with methanol. The eluent was dried *in vacuo*. The crude extract
505 was resuspended with methanol and fractionated using the Sephadex LH-20 column.
506 Fractions containing the target peaks were combined and further purified by Semiprep HPLC
507 with a C18 Preparative Cartridge (Agilent, 5 µm, 21.2 x 150 mm). A gradient method (55%
508 acetonitrile-water to 85% acetonitrile-water in 12 mins, 10 mL min^{-1}) was applied for the
509 separation of peak III with peaks I-III.

510 For structural characterisation of **1** and **2**, nuclear magnetic resonance (NMR) spectra were
511 collected on Bruker Avance IIIHD 500/600MHz NMR spectrometers, with either CDCl3-*d* or
512 MeOD-d_4 as solvents. NMR data in $CDCl_3$ was in good agreement with the published data
513 (Supplementary Table 2; Supplementary Table 3)

514 **Computational analysis of *A. nidulans* features**

515 The genome assembly and corresponding gene annotations for *A. nidulans* FGSC A4 were
516 obtained from FungiDB (denoted version 46) [33] Coordinates of predicted BGCs were obtained
517 from the *A. nidulans* portal on the Joint Genome Institute's MycoCosm resource[58]. The
518 genome was parsed for gene features using Python scripts. Genes falling within cluster
519 boundaries were grouped, forming an additional dataset to facilitate comparison between the
520 whole genome and BGC genes.

521 Lengths of 5′ UTRs were determined for all genes and BGC genes, based on features when
522 available, filtering the genes with 5′ UTRs equal zero. Histograms for each dataset were
523 plotted using the Matplotlib library.
524 To determine the frequency of Cas9 and Cas12a PAM sites, upstream regions for all genes
525 were isolated by taking up to 400 bp upstream of the start codon. When intergenic distance
526 was less than 400 bp, the distance between the start codon and the end of the previous gene
527 was used. Frequencies of the different PAM sites were obtained through regular expression
528 searches of the PAM sequences considering both strands. Histograms for each dataset were
529 plotted as mentioned above.

530 **Statistical analysis**

531 Statistical analysis was done using GraphPad Prism 8.3.0. All data were analysed with three
532 biological replicates and Two-sided Welch's T-test with Holm-Šídák multiplicity correction per
533 figure, using an alpha of 0.05. All Welch's T-test P-values calculated for each experiment along
534 the details for the multiplicity adjustment are found in Supplementary Table 9.

535 Acknowledgements

536 Y.H.C. and this project is supported by an ARC Future Fellowship (FT160100233). I.R. is
537 recipient of an UWA PhD Scholarship, J.H. and C.L.M.G. on Australian Government Research
538 Training Program Scholarships. NMR and LC-MS/MS were performed at the UWA Centre for
539 Microscopy, Characterisation and Analysis (CMCA). We thank Berl Oakley for *A. nidulans*
540 LO8030 strain, and Christian Pflüger and Andrew Piggott for helpful discussion.

541 Data Availability

542 All relevant data generated during this study are available from the corresponding author on
543 reasonable request. Main plasmids will be made available in Addgene, other plasmids are
544 available under request.

545 Code Availability

546 All Python code used in these analyses is implemented in a Jupyter notebook which is
547 available at https://github.com/gamcil/5_UTR_analysis/ alongside accompanying data.

548 Competing interests

549 The authors declare no competing interests.

Author contributions

I.R and Y.H.C conceived the project. I.R., C.W. and Y.H.C. wrote the manuscript. I.R. designed the constructs. I.R., C.W. and R.W. contributed to cloning. I.R. and C.W. performed the experiments and the data analysis. J.H. performed the NMR structural elucidation. C.L.M.G. wrote the code for computational analysis.

References

1. Keller, N. P. Fungal secondary metabolism: regulation, function and drug discovery. *Nature Reviews Microbiology* **17,** 167–180 (2019).
2. Rutledge, P. J. & Challis, G. L. Discovery of microbial natural products by activation of silent biosynthetic gene clusters. *Nature Reviews Microbiology* **13,** 509–523 (2015).
3. Rokas, A., Wisecaver, J. H. & Lind, A. L. The birth, evolution and death of metabolic gene clusters in fungi. *Nature Reviews Microbiology* **16,** 731–744 (2018).
4. Pfannenstiel, B. T. & Keller, N. P. On top of biosynthetic gene clusters: How epigenetic machinery influences secondary metabolism in fungi. *Biotechnology Advances* **37,** 1–14 (2019).
5. Alberti, F., Foster, G. D. & Bailey, A. M. Natural products from filamentous fungi and production by heterologous expression. *Appl. Microbiol. Biotechnol.* **101,** 493–500 (2017).
6. Kjærbølling, I., Mortensen, U. H., Vesth, T. & Andersen, M. R. Strategies to establish the link between biosynthetic gene clusters and secondary metabolites. *Fungal Genetics and Biology* **130,** 107–121 (2019).
7. Gilchrist, C. L. M., Li, H. & Chooi, Y. H. Panning for gold in mould: Can we increase the odds for fungal genome mining? *Org. Biomol. Chem.* **16,** 1620–1626 (2018).
8. Yeh, H. H. *et al.* Resistance Gene-Guided Genome Mining: Serial Promoter Exchanges in Aspergillus nidulans Reveal the Biosynthetic Pathway for Fellutamide B, a Proteasome Inhibitor. *ACS Chem. Biol.* **11,** 2275–2284 (2016).
9. Bergmann, S. *et al.* Genomics-driven discovery of PKS-NRPS hybrid metabolites from Aspergillus nidulans. *Nat. Chem. Biol.* **3,** 213–217 (2007).
10. Grau, M. F. *et al.* Hybrid Transcription Factor Engineering Activates the Silent Secondary Metabolite Gene Cluster for (+)-Asperlin in Aspergillus nidulans. *ACS Chem. Biol.* **13,** 3193–3205 (2018).
11. He, Y. *et al.* Recent advances in reconstructing microbial secondary metabolites biosynthesis in Aspergillus spp. *Biotechnol. Adv.* **36,** 739–783 (2018).
12. Clevenger, K. D. *et al.* A scalable platform to identify fungal secondary metabolites and their gene clusters. *Nat. Chem. Biol.* **13,** 895–901 (2017).
13. Chiang, Y. M. *et al.* An efficient system for heterologous expression of secondary metabolite genes in Aspergillus nidulans. *J. Am. Chem. Soc.* **135,** 7720–7731 (2013).
14. Liu, L., Tang, M.-C. & Tang, Y. Fungal Highly Reducing Polyketide Synthases Biosynthesize Salicylaldehydes that are Precursors to Epoxycyclohexenol Natural Products. *J. Am. Chem. Soc.* **141,** 19538–19541 (2019).
15. Hu, J. *et al.* Heterologous biosynthesis of elsinochrome A sheds light on the formation of the photosensitive perylenequinone system. *Chem. Sci.* **10,** 1457–1465 (2019).
16. Li, H. *et al.* Genomics-Driven Discovery of Phytotoxic Cytochalasans Involved in the Virulence of the Wheat Pathogen Parastagonospora nodorum. *ACS Chem. Biol.* (2019). doi:10.1021/acschembio.9b00791
17. Dominguez, A. A., Lim, W. A. & Qi, L. S. Beyond editing: Repurposing CRISPR-Cas9 for precision genome regulation and interrogation. *Nat. Rev. Mol. Cell Biol.* **17,** 5–15 (2016).
18. Chavez, A. *et al.* Highly efficient Cas9-mediated transcriptional programming. *Nat. Methods* **12,** 326–328 (2015).

600 19. Tak, Y. E. *et al.* Inducible and multiplex gene regulation using CRISPR-Cpf1-based
601 transcription factors. *Nat. Methods* **14,** 1163–1166 (2017).
602 20. Zalatan, J. G. *et al.* Engineering complex synthetic transcriptional programs with
603 CRISPR RNA scaffolds. *Cell* **160,** 339–350 (2015).
604 21. Peng, R. *et al.* CRISPR/dCas9-mediated transcriptional improvement of the
605 biosynthetic gene cluster for the epothilone production in Myxococcus xanthus.
606 *Microb. Cell Fact.* **17,** 1–12 (2018).
607 22. Deaner, M. & Alper, H. S. Systematic testing of enzyme perturbation sensitivities via
608 graded dCas9 modulation in Saccharomyces cerevisiae. *Metab. Eng.* **40,** 14–22
609 (2017).
610 23. Schwartz, C., Curtis, N., Löbs, A. K. & Wheeldon, I. Multiplexed CRISPR Activation of
611 Cryptic Sugar Metabolism Enables Yarrowia Lipolytica Growth on Cellobiose.
612 *Biotechnol. J.* **13,** 1–7 (2018).
613 24. Aleksenko, A. & Clutterbuck, A. J. Autonomous plasmid replication in Aspergillus
614 nidulans AMA1 and MATE elements. *Fungal Genet. Biol.* **21,** 373–387 (1997).
615 25. Chiang, Y. M. *et al.* Development of Genetic Dereplication Strains in Aspergillus
616 nidulans Results in the Discovery of Aspercryptin. *Angew. Chemie - Int. Ed.* **55,** 1662–
617 1665 (2016).
618 26. Chooi, Y. H. *et al.* Functional genomics-guided discovery of a light-activated
619 phytotoxin in the wheat pathogen Parastagonospora nodorum via pathway activation.
620 *Environ. Microbiol.* **19,** 1975–1986 (2017).
621 27. Fonfara, I., Richter, H., BratoviÄ, M., Le Rhun, A. & Charpentier, E. The CRISPR-
622 associated DNA-cleaving enzyme Cpf1 also processes precursor CRISPR RNA.
623 *Nature* **532,** 517–521 (2016).
624 28. Zhong, G., Wang, H., Li, Y., Tran, M. H. & Farzan, M. Cpf1 proteins excise CRISPR
625 RNAs from mRNA transcripts in mammalian cells. *Nat. Chem. Biol.* **13,** 839–841
626 (2017).
627 29. Pall, M. L. & Brunelli, J. P. A series of six compact fungal transformation vectors
628 containing polylinkers with multiple unique restriction sites. *Fungal Genet. Rep.* **40,**
629 59–62 (1993).
630 30. Nødvig, C. S. *et al.* Efficient oligo nucleotide mediated CRISPR-Cas9 gene editing in
631 Aspergilli. *Fungal Genet. Biol.* **115,** 78–89 (2018).
632 31. Yeh, H. H. *et al.* Molecular genetic analysis reveals that a nonribosomal peptide
633 synthetase-like (NRPS-like) gene in Aspergillus nidulans is responsible for
634 microperfuranone biosynthesis. *Appl. Microbiol. Biotechnol.* **96,** 739–748 (2012).
635 32. Sibthorp, C. *et al.* Transcriptome analysis of the filamentous fungus Aspergillus
636 nidulans directed to the global identification of promoters. *BMC Genomics* **14,** 847
637 (2013).
638 33. Basenko, E. Y. *et al.* FungiDB: An integrated bioinformatic resource for fungi and
639 oomycetes. *J. Fungi* **4,** (2018).
640 34. Jensen, M. K. Design principles for nuclease-deficient CRISPR-based transcriptional
641 regulators. *FEMS Yeast Res.* **18,** 1–11 (2018).
642 35. Andersen, M. R. *et al.* Accurate prediction of secondary metabolite gene clusters in
643 filamentous fungi. *Proc. Natl. Acad. Sci.* **110,** E99–E107 (2012).
644 36. Hamasaki, T., Nakajima, H., Yokota, T. & Kimura, Y. A New Metabolite, 3-Carboxy-
645 2,4-diphenyl-but-2-enoic Anhydride, Produced by Aspergillus nidulans. *Agric. Biol.*
646 *Chem.* **47,** 891–892 (1983).
647 37. Allen, F., Pon, A., Wilson, M., Greiner, R. & Wishart, D. CFM-ID: A web server for
648 annotation, spectrum prediction and metabolite identification from tandem mass
649 spectra. *Nucleic Acids Res.* **42,** (2014).
650 38. Oakley, C. E. *et al.* Discovery of McrA, a master regulator of Aspergillus secondary
651 metabolism. *Mol. Microbiol.* **103,** 347–365 (2017).
652 39. Moreno-Mateos, M. A. *et al.* CRISPR-Cpf1 mediates efficient homology-directed
653 repair and temperature-controlled genome editing. *Nat. Commun.* **8,** 2024 (2017).
654 40. Dix, N. J., Webster, J., Dix, N. J. & Webster, J. Fungi of Extreme Environments. in

655 *Fungal Ecology* 322–340 (1995). doi:10.1007/978-94-011-0693-1_12
656 41. Kleinstiver, B. P. *et al.* Engineered CRISPR–Cas12a variants with increased activities
657 and improved targeting ranges for gene, epigenetic and base editing. *Nat. Biotechnol.*
658 **37**, 276–282 (2019).
659 42. Yamano, T. *et al.* Crystal Structure of Cpf1 in Complex with Guide RNA and Target
660 DNA. *Cell* **165,** 949–962 (2016).
661 43. Yamano, T. *et al.* Structural Basis for the Canonical and Non-canonical PAM
662 Recognition by CRISPR-Cpf1. *Mol. Cell* **67,** 633–645.e3 (2017).
663 44. Zetsche, B. *et al.* Cpf1 Is a Single RNA-Guided Endonuclease of a Class 2 CRISPR-
664 Cas System. *Cell* **163,** 759–771 (2015).
665 45. Joung, J. K., Kleinstiver, B. & Sousa, A. Variants of CPF1 (CAS12a) With Altered
666 PAM Specificity. US patent 20190010481A1 (2019).
667 46. Sanson, K. R. *et al.* Optimized libraries for CRISPR-Cas9 genetic screens with
668 multiple modalities. *Nat. Commun.* **9,** 5416 (2018).
669 47. Campa, C. C., Weisbach, N. R., Santinha, A. J., Incarnato, D. & Platt, R. J.
670 Multiplexed genome engineering by Cas12a and CRISPR arrays encoded on single
671 transcripts. *Nat. Methods* **16**, 887–893 (2019).
672 48. Nihongaki, Y., Otabe, T., Ueda, Y. & Sato, M. A split CRISPR–Cpf1 platform for
673 inducible genome editing and gene activation. *Nat. Chem. Biol.* **15,** 882–888 (2019).
674 49. Howe, F. S. *et al.* CRISPRi is not strand-specific at all loci and redefines the
675 transcriptional landscape. *Elife* **6**, e29878 (2017).
676 50. Schindele, P. & Puchta, H. Engineering CRISPR/LbCas12a for highly efficient,
677 temperature-tolerant plant gene editing. *Plant Biotechnology Journal* (2019).
678 doi:10.1111/pbi.13275
679 51. Tsunematsu, Y. *et al.* Distinct mechanisms for spiro-carbon formation reveal
680 biosynthetic pathway crosstalk. *Nat. Chem. Biol.* **9,** 818–825 (2013).
681 52. Chooi, Y. H. *et al.* Genome mining of a prenylated and immunosuppressive polyketide
682 from pathogenic fungi. *Org. Lett.* **15,** 780–783 (2013).
683 53. Zetsche, B. *et al.* Multiplex gene editing by CRISPR-Cpf1 using a single crRNA array.
684 *Nat. Biotechnol.* **35,** 31–34 (2017).
685 54. Boyce, K. J., Bugeja, H. E., Weerasinghe, H., Payne, M. J. & Schreider, L. Strategies
686 for the molecular genetic manipulation and visualization of the human fungal
687 pathogen Penicillium marneffei. *Fungal Genet. Rep.* **59,** 1–12 (2012).
688 55. Cerqueira, G. C. *et al.* The Aspergillus Genome Database: Multispecies curation and
689 incorporation of RNA-Seq data to improve structural gene annotations. *Nucleic Acids*
690 *Res.* **42,** 705–710 (2014).
691 56. Tarleton, R. & Peng, D. EuPaGDT: a web tool tailored to design CRISPR guide RNAs
692 for eukaryotic pathogens. *Microb. Genomics* **1,** 1–7 (2015).
693 57. Lim, F. Y., Sanchez, J. F., Wang, C. C. C. & Keller, N. P. Toward awakening cryptic
694 secondary metabolite gene clusters in filamentous fungi. *Methods Enzymol.* **517,**
695 303–324 (2012).
696 58. Grigoriev, I. V. *et al.* MycoCosm portal: Gearing up for 1000 fungal genomes. *Nucleic*
697 *Acids Res.* **42,** (2014).
698
699

700 # Supplementary Information

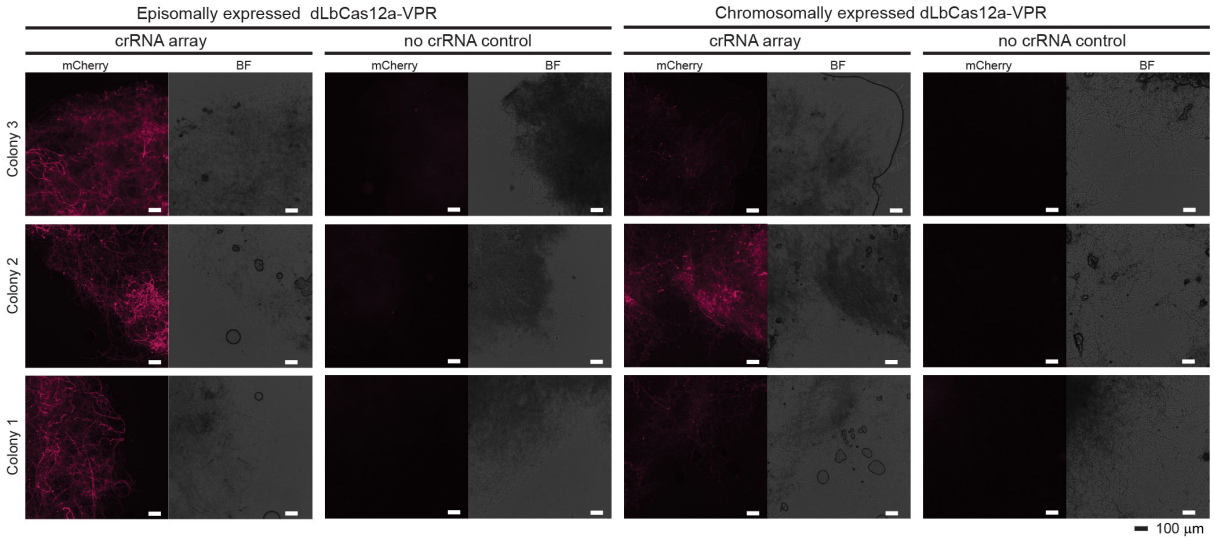

701

702 **Supplementary Fig. 1:** Activation of the fluorescent reporter P_{elcA}-*mCherry* by
703 CRISPR/dLbCas12a-VPR. Fluorescence microscopy images of *A. nidulans* mycelia
704 demonstrate mCherry fluorescence when the poly-crRNA array is present in both episomally
705 and chromosomally expressed dLbCas12a-VPR systems, distinct from the no crRNA control.
706 The spores for each sample were collected from three individual colonies and grown overnight
707 in liquid stationary culture at 37 °C. Samples with similar mycelial growth were observed under
708 mCherry filter and brightfield (BF). Scale bar 100 µm.

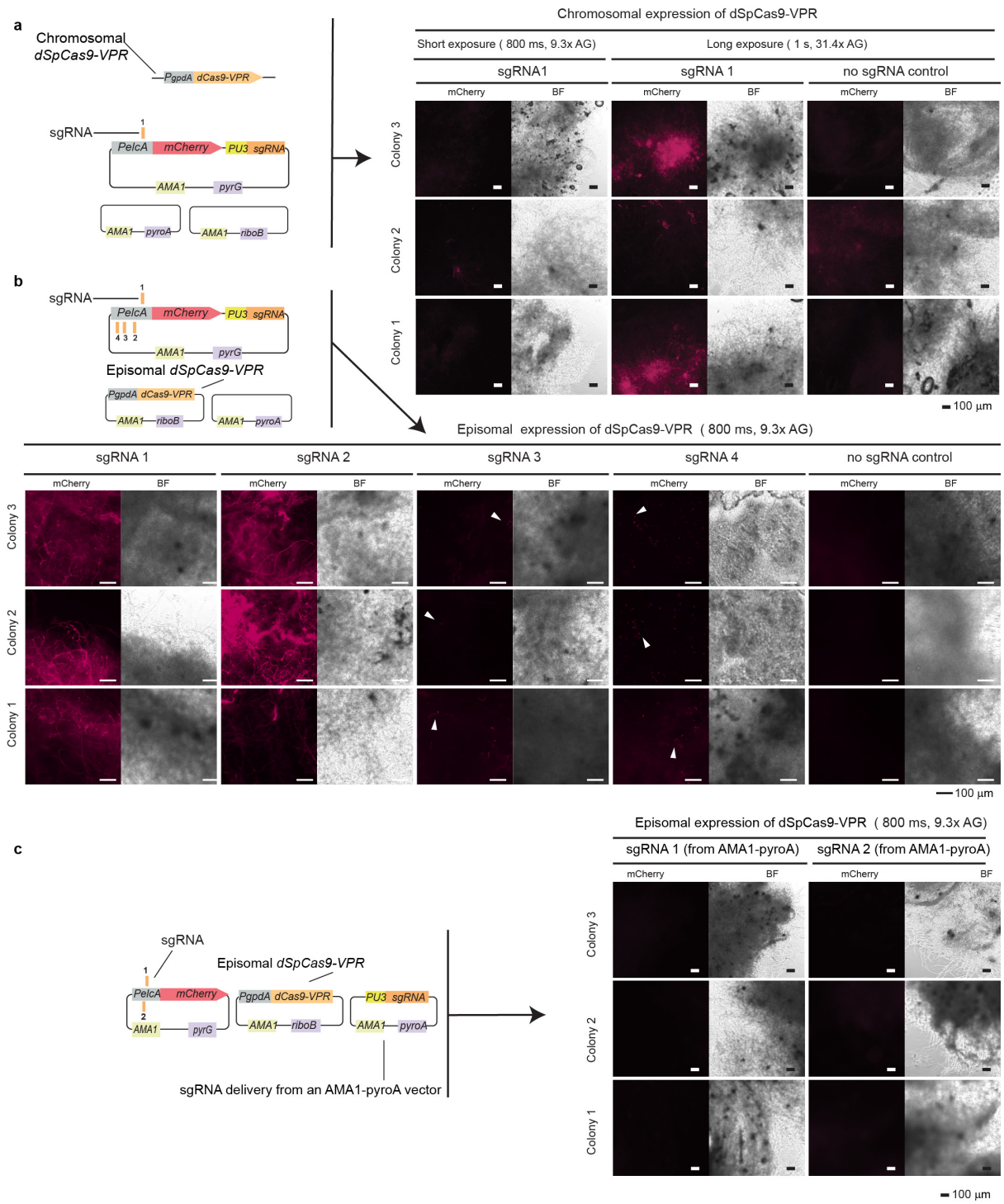

Supplementary Fig. 2. Activation of the fluorescent reporter P_{elcA}-*mCherry* by CRISPR/dSpCas9-VPR is dependent on CRISPRa components mode of delivery**. a.** CRISPRa samples with dSpCas9-VPR is chromosomally expressed and sgRNA 1(presented in diagram) resulted in low activation the mcherry reporter, although samples were distinct to the no sgRNA control when observed at prolonged exposure times and increased sensitivity (1s exposure and 31.4x analog gain). **b.** AMA1-encoded CRISPR/dSpCas9-VPR system (presented diagrammatically) resulted in strong fluorescence observable in all mycelia at short exposure times when targeting the reporter construct with sgRNA 1 or sgRNA 2. The two

718 sgRNA targeting regions further away from the gene start codon (sgRNA 3 and sgRNA 4)
719 resulted in low fluorescence localized in spores or isolated mycelia, but distinguishable from
720 the no sgRNA negative control. Images are 2X digitally zoomed to show the fluorescence of
721 the spores (white arrows). **c.** The strong activation by the episomally delivered dSpCas9-VPR
722 system observed with sgRNA 1 and sgRNA 2 is abolished when the sgRNA is delivered
723 encoded in a separate AMA1-pyro vector (represented in adjacent diagram). The spores for
724 each sample were collected from three individual colonies and grown overnight in liquid
725 stationary culture at 37 °C. Samples with similar mycelial growth were observed under
726 mCherry filter and brightfield (BF). Scale bar 100 μm.

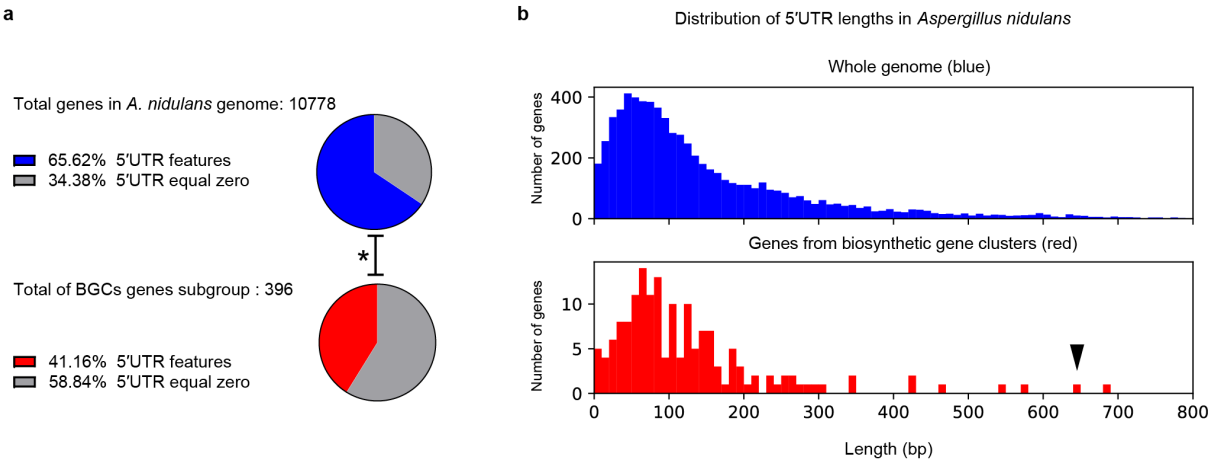

727
728

729 **Supplementary Fig. 3.** *Aspergillus nidulans* 5′ UTR features **a.** Access to transcription starting
730 site (TSS) information for CRISPRa targeting is limited in the current version of the *A. nidulans*
731 genome. The proportion of genes that have annotated 5′ UTR lengths greater than zero is
732 smaller for BGCs compared to the whole genome. This could be due to the low expression of
733 most BGCs genes in the growth conditions in which the transcriptomic data was acquired [1].
734 Asterisk represents the significant result of Fisher's exact test two-sided $p<0.0001$. **b.**
735 Distribution of 5′ UTR length in *Aspergillus nidulans* genes for the whole genome (blue) and
736 in genes that fall within BGC boundaries only (red), after filtering genes with no 5′ UTR
737 annotation. Arrow indicates the *micA* 5′ UTR length.

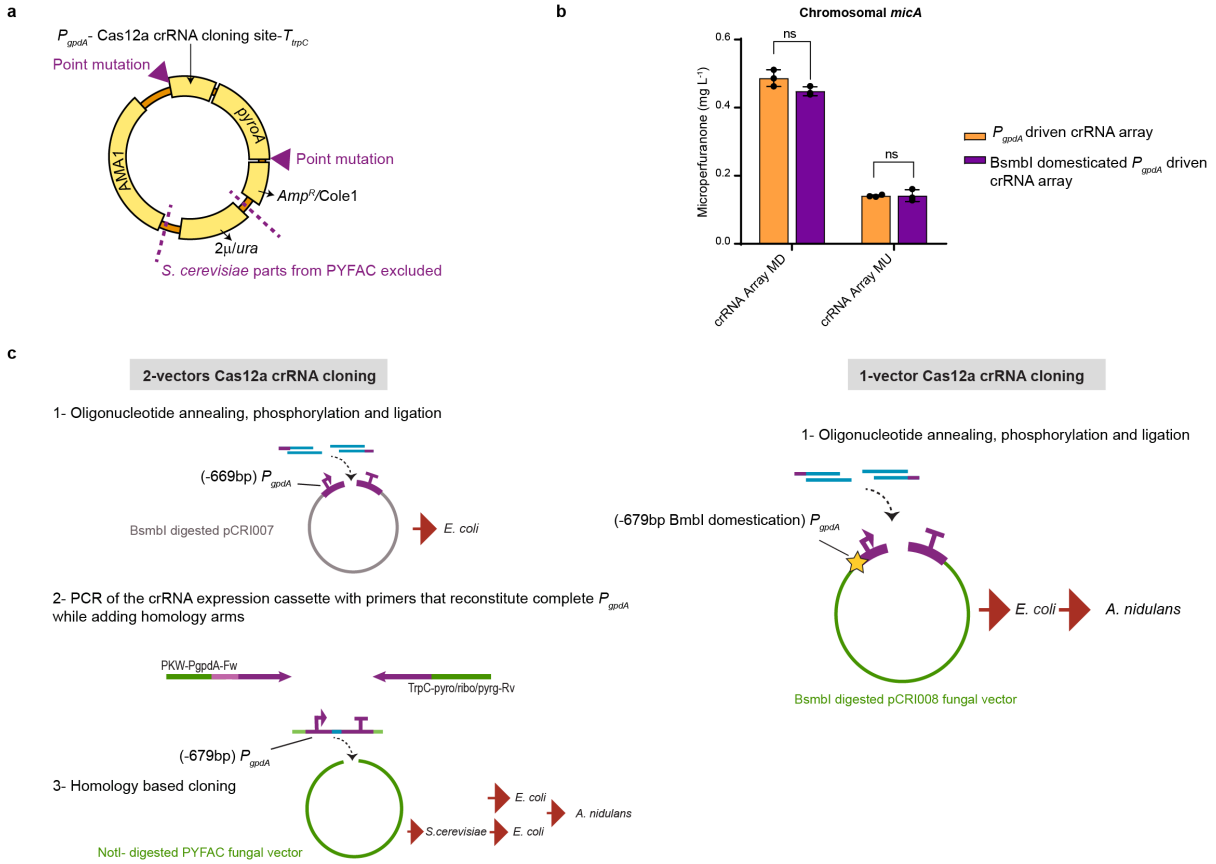

Supplementary Fig. 4 . One-step cloning of Cas12a crRNA with pCRI008. **A.** Diagram of the BsmbI domestication strategy used to create the vector pCRI008. Two point mutations were introduced, one in P_{gpdA} promoter from the crRNA expression cassette, and the other in the *pyroA* marker terminator region. The components of pYFAC for replication in *Saccharomyces cerevisiae* were eliminated to avoid BsmbI sites. **b.** No difference in microperfuranone (**1**) activation mediated by CRISPRa is observed between systems with crRNA array expression driven by the original P_{gpdA} sequence (orange) and the BsmbI domesticated version of P_{gpdA} (purple), confirming the null effect of the mutation. Titres of **1** (mg L^{-1}) values are the mean of three biological replicates, specific values of which are indicated as black dots, bars represent SD. Two-sided Welch's T-test was performed. Asterisk indicates P-value<0.05. Individual P-values are listed in Supplementary Table 9. **c.** The simplified one-vector cloning strategy with the BsmbI-domesticated pCRI008 versus the original two-vector cloning strategy. In the two-vector strategy, a shorter P_{gpdA} lacking BsmbI site was cloned into a pGEM-T backbone to create a vector (pCRI007) for type IIS restriction enzyme cloning. This crRNA cassette would be later be amplified by primers that would reconstitute the full P_{gpdA} sequence when incorporated into a fungal vector by homology-based cloning.

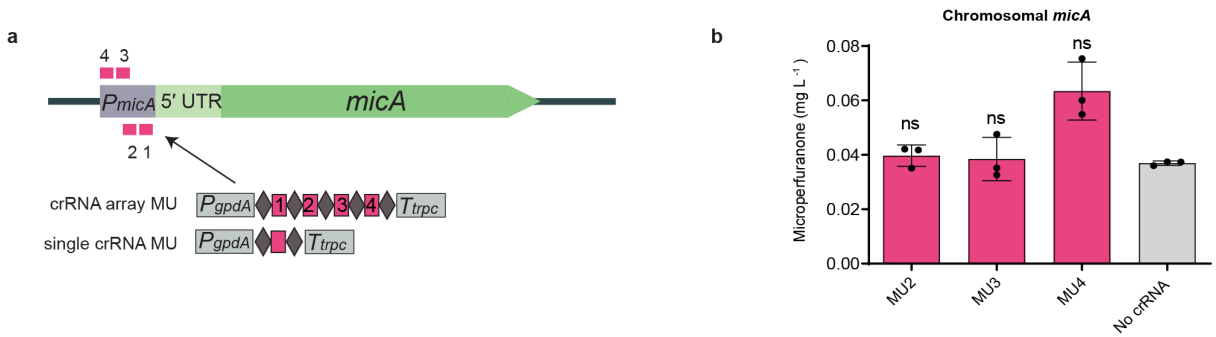

Supplementary Fig. 5. Individual MU crRNA tested do not result in significant activation. **a.** Chromosomal *micA* gene scheme with individual crRNA MU (magenta) target sites indicated. Numbers assigned to crRNA MD are indicative of targeting position in respect to *micA* TSS, with their position in the crRNA array MD also indicated in the scheme **b.** No significant changes in the production of microperfuranone are observed targeting with single crRNAs compared to the no crRNA control. Microperfuranone titre (mg L^{-1}) values are the mean of three biological replicates in which specific values are indicated as black dots, error bars represent SD. Two-sided Welch's T-test with Holm-Šídák multiplicity correction per figure was performed. Asterisk indicates corrected P-value<0.05. Individual P-values are listed in Supplementary Table 9.

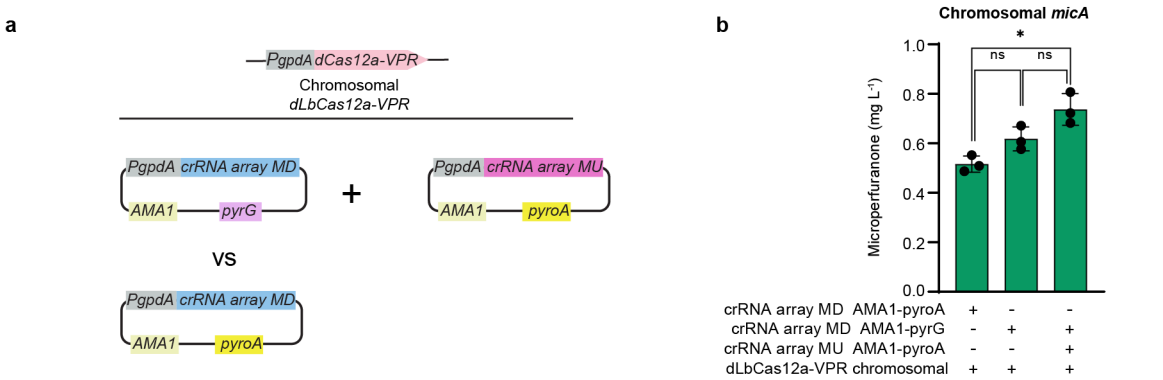

Supplementary Fig. 6. CRISPRa of *micA* with both MD and MU crRNA arrays. **a.** Overview of double crRNA array mediated activation of *micA* in strains harbouring chromosomally integrated *dLbCas12a-VPR*. In order to allow co-transformation of two crRNA arrays, crRNA array MD was re-cloned into an AMA1-pyrG vector. This allowed comparing the performance of crRNA array MD in both AMA1-pyrG and AMA1-pyroA vectors. **b.** Double crRNA array (8 crRNA) mediated activation of *micA* resulted in microperfuranone titres higher than the four-crRNA array MD alone when delivered from AMA1-pyroA. However, there is no significant increase from the production observed by crRNA array MD alone when delivered from AMA1-pyrG. The differences in the production mediated by crRNA MD when using the markers *pyrG* and *pyroA* is not significant, suggests that the marker used for crRNA delivery might influence the system performance. Microperfuranone titre (mg L^{-1}) values are the mean of three biological replicates, of which specific values are indicated as black dots, bars represent SD.

780 Two-sided Welch's T-test with Holm-Šídák multiplicity correction per figure was performed.
781 Asterisk indicates corrected P-value<0.05, (ns) not significant. Individual P-values are listed
782 in Supplementary Table 9.

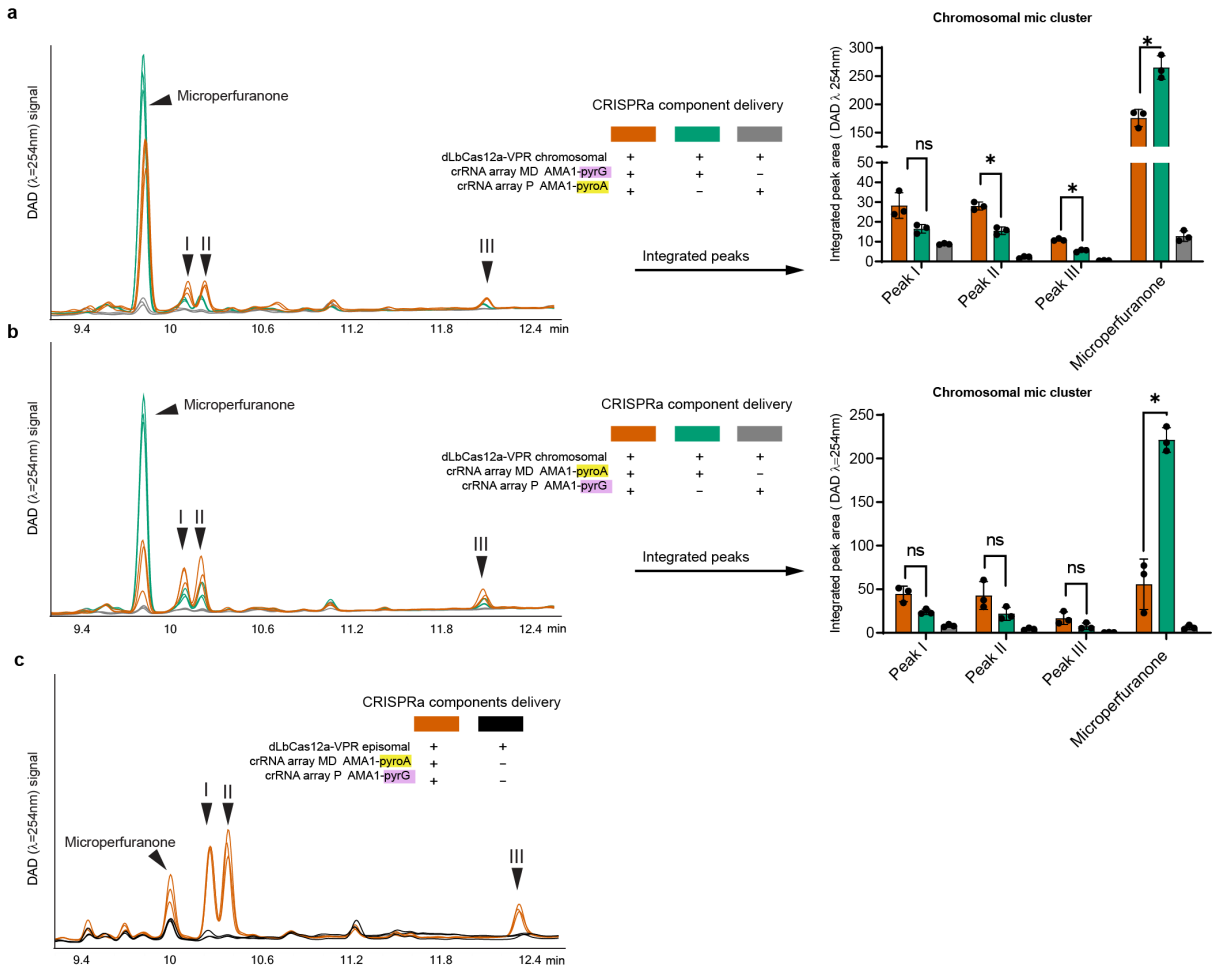

783

784 **Supplementary Fig. 7.** Multiple gene activation of *mic* cluster.**a–b.** Overlaid DAD (λ=254 nm)
785 chromatograms of acidified ethyl acetate mix media crude extracts from strains co-
786 transformed with the multiple crRNA arrays MD and P (orange), crRNA array MD (green) and
787 crRNA array P (grey) strains; combination in **a** for multiple targeting (orange), crRNA MD in
788 AMA1-pyrG and crRNA P in AMA1-pyroA; combination in for **b** (orange), crRNA MD in AMA1-
789 pyroA and crRNA P in AMA1-pyrG. Both multiple crRNA arrays (orange) for combinations **a**
790 and **b** showed conversion of the precursor microperfuranone to the peaks I–III. Compared to
791 **a**, combination **b** showed a stronger decrease in the titre of the precursor microperfuranone
792 and higher titre of the peaks I–III. **c.** Expression of dLbCas12a-VPR from the multicopy AMA1-
793 vector with the same crRNA array delivery combination as **b** resulted in a further increase of
794 peaks I–III production relative to microperfuranone. Chromatograms in **a**,**b**,**c** are represented
795 at the same scale. Microperfuranone titre (mg L^{-1}) values are the mean of three biological
796 replicates, of which specific values are indicated as black dots, bars represent SD. Two-sided
797 Welch's T-test with Holm-Šídák multiplicity correction per figure was performed. Asterisk

798 indicates corrected P-value<0.05, (ns) not significant. Individual P-values are listed in
799 Supplementary Table 9.

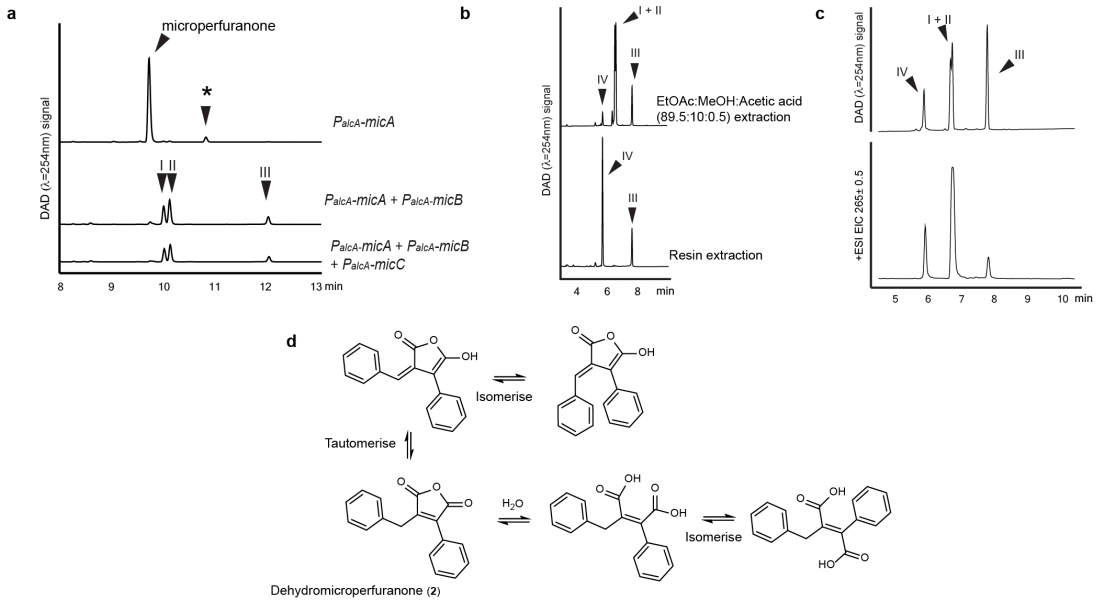

800

801 **Supplementary Fig. 8.** Verification of *mic* cluster product by promoter exchange and
802 dehydromicroperfuranone isolation. **a.** DAD (λ=254 nm) chromatograms from *mic* cluster
803 genes (*micA*–*C*) expression from an alcohol inducible promoter (P_{alcA}). Overexpression of
804 *micA* results in the expected microperfuranone peak and a smaller unidentified peak likely to
805 be a side product of microperfuranone with m/z 251 (asterisk). Co-expression of *micA* and
806 *micB* resulted in the production of the peaks I–III peaks as expected. Co-expression of *micA*–
807 *C* results in the same metabolic profile of *micA*–*B*, indicating that *micC* is likely not necessary
808 to produce peaks I–III. All chromatograms run with a gradient of 20 min. **b.** Metabolic profile
809 of highly concentrated samples from culture media crude extract obtained when scaling up for
810 purification showing peaks I–III and a smaller IV of identical *m*/*z* 265 when extracted with
811 acidified ethyl acetate and methanol mix. When extracting the same media with a solid resin
812 we observe only the peaks IV and III. All chromatograms with a gradient of 10 min. **c.** LC-
813 DAD-MS analysis of the purified peak III used for NMR analysis (top, DAD chromatogram
814 λ=254 nm; bottom, extracted ion chromatogram m/z 265). The purified peak III NMR sample
815 in chloroform-*d*, which appeared as a pure single chemical entity based on ^{1}H and ^{13}C NMR
816 analysis (Supplementary Table 2, Supplementary Fig. 9 and 10), was dried and reconstituted
817 in methanol for the LC-DAD-MS analysis. LC-DAD-MS of co-purified peaks I–II shared the
818 same profile. ^{1}H NMR analysis of the reconstituted sample in methanol-*d* also showed that the
819 compounds existed as mixed forms (Supplementary Fig. 13 and 14). **d.** Possible
820 interconvertible forms of dehydromicroperfuranone based on possible tautomerisation and *cis*-
821 *trans* isomerisation of maleic acid to fumaric acid. Note: *m*/z 283 was occasionally observed

822 to coexist with *m*/*z* 265 for the peaks I–IV suggesting that some of the *m*/*z* 265 ions detected
823 could be $[M+H-H_2O]^+$. However, it is difficult to determine which peaks is in which form as they
824 appear as a single peak in chloroform-*d* during NMR analysis and converted back to multiple
825 peaks during LC-DAD-MS.
826

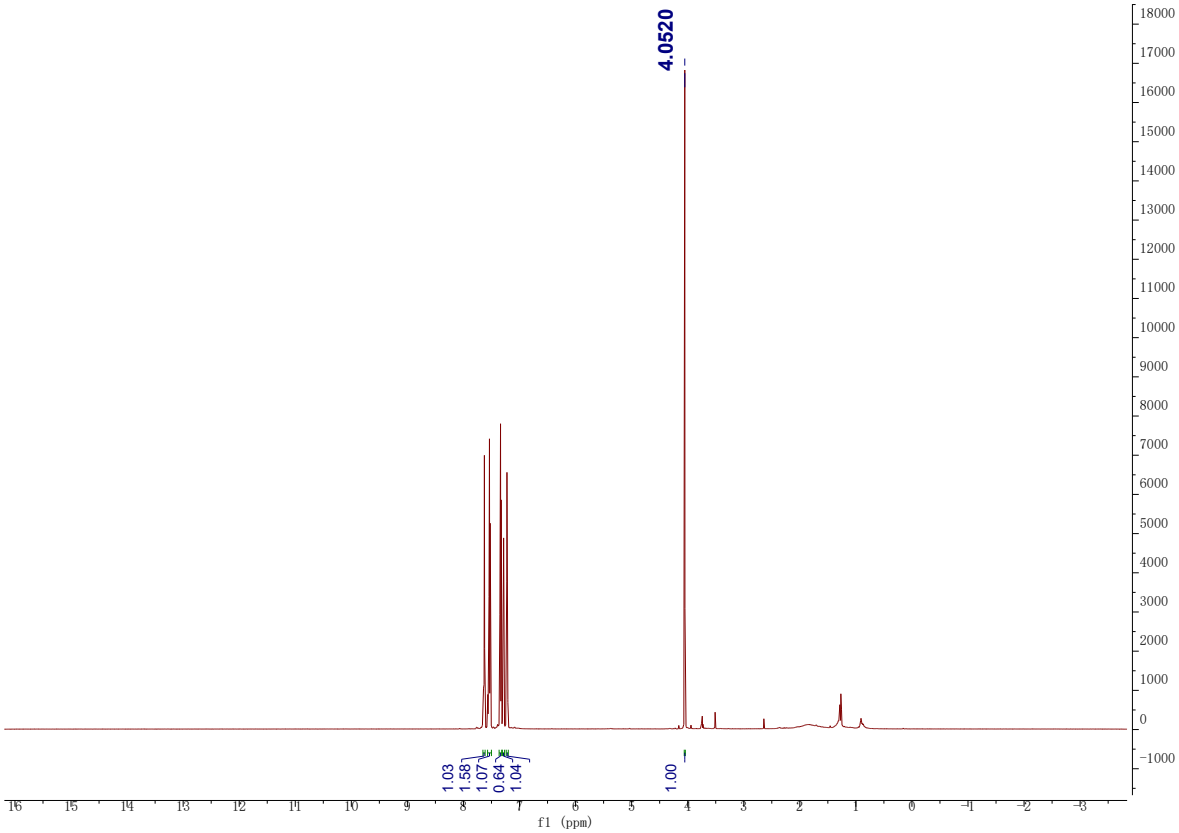

Supplementary Fig. 9 ^{1}H NMR spectrum (600 MHz) of purified peak III in $CDCl_3$-*d*.

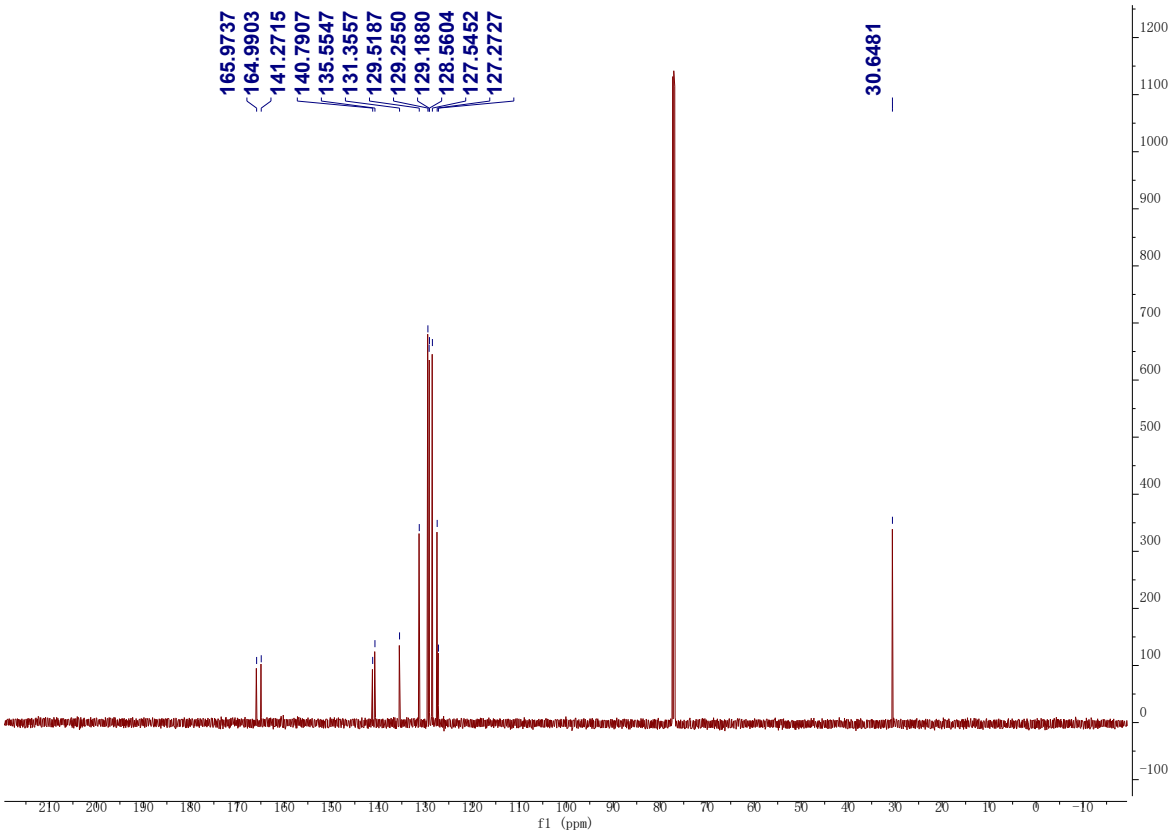

Supplementary Fig. 10 ^{13}C NMR spectrum (150 MHz) of purified peak III in $CDCl_3$-*d*.

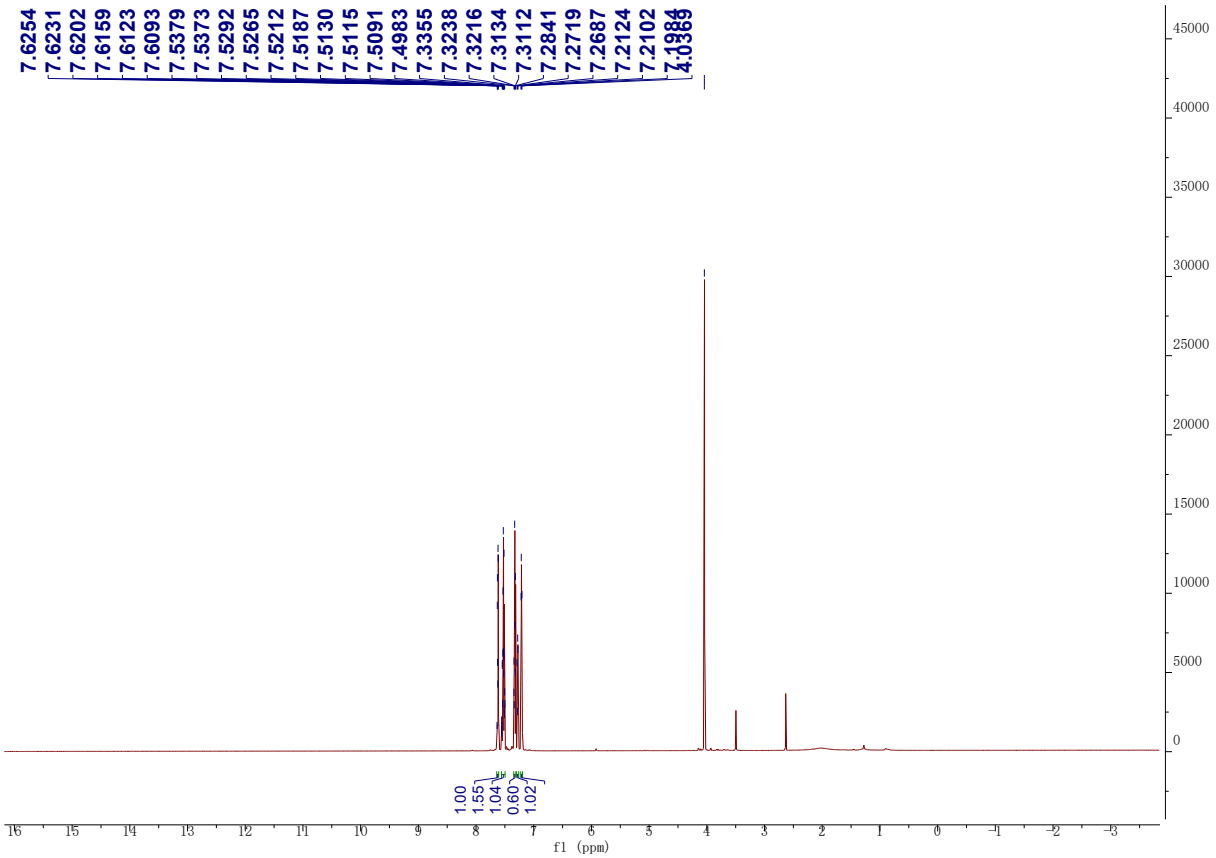

Supplementary Fig. 11 ^{1}H NMR spectrum (600 MHz) of purified peals I-II in $CDCl_3$-*d*.

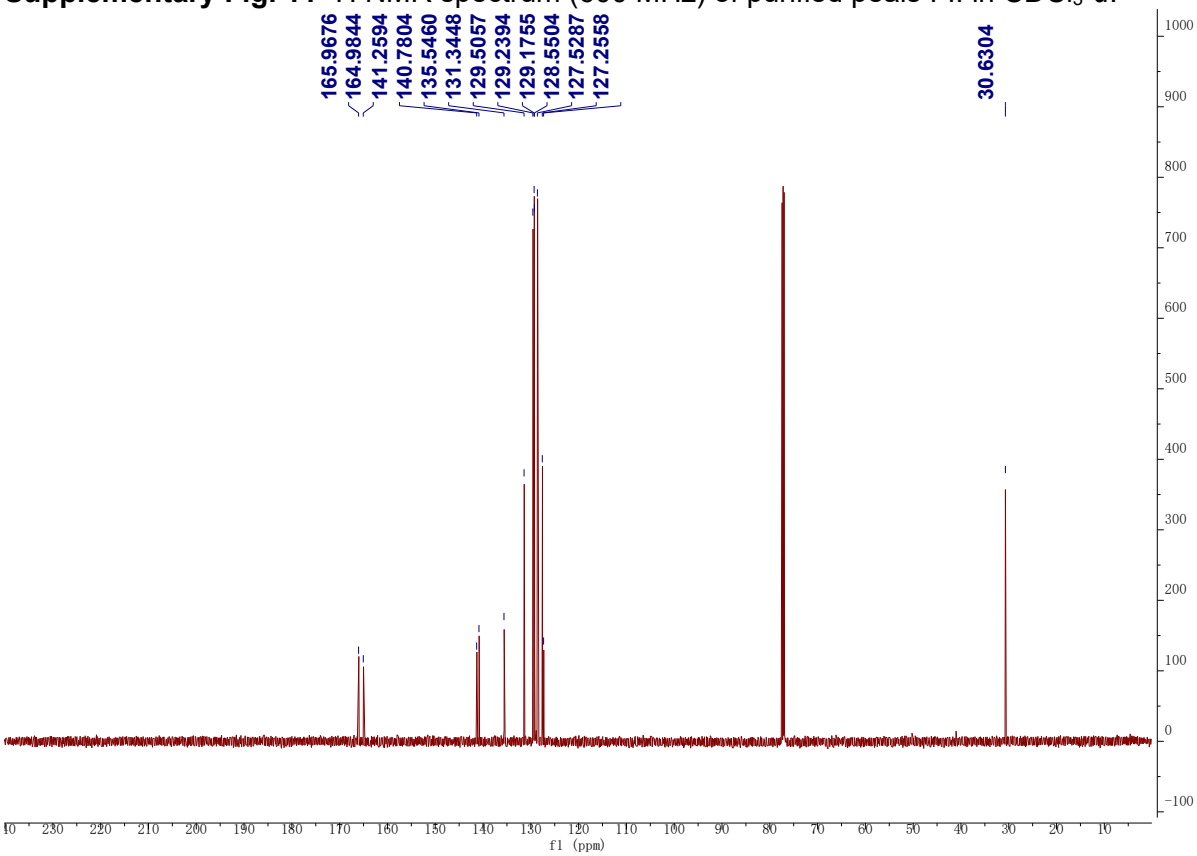

Supplementary Fig. 12 ^{13}C NMR spectrum (150 MHz) of purified peaks I-II in $CDCl_3$-*d*.

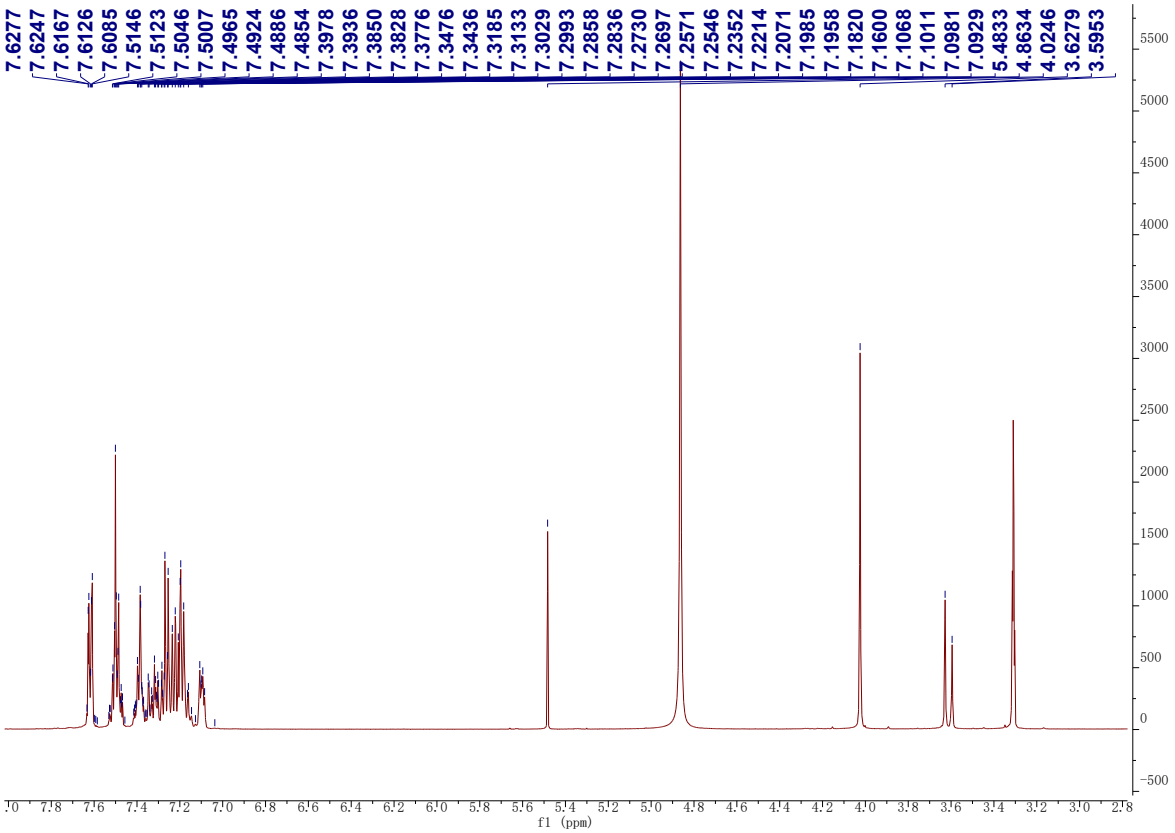

Supplementary Fig. 13. ^{1}H NMR of purified peaks I-II in MeOD (500MHz)

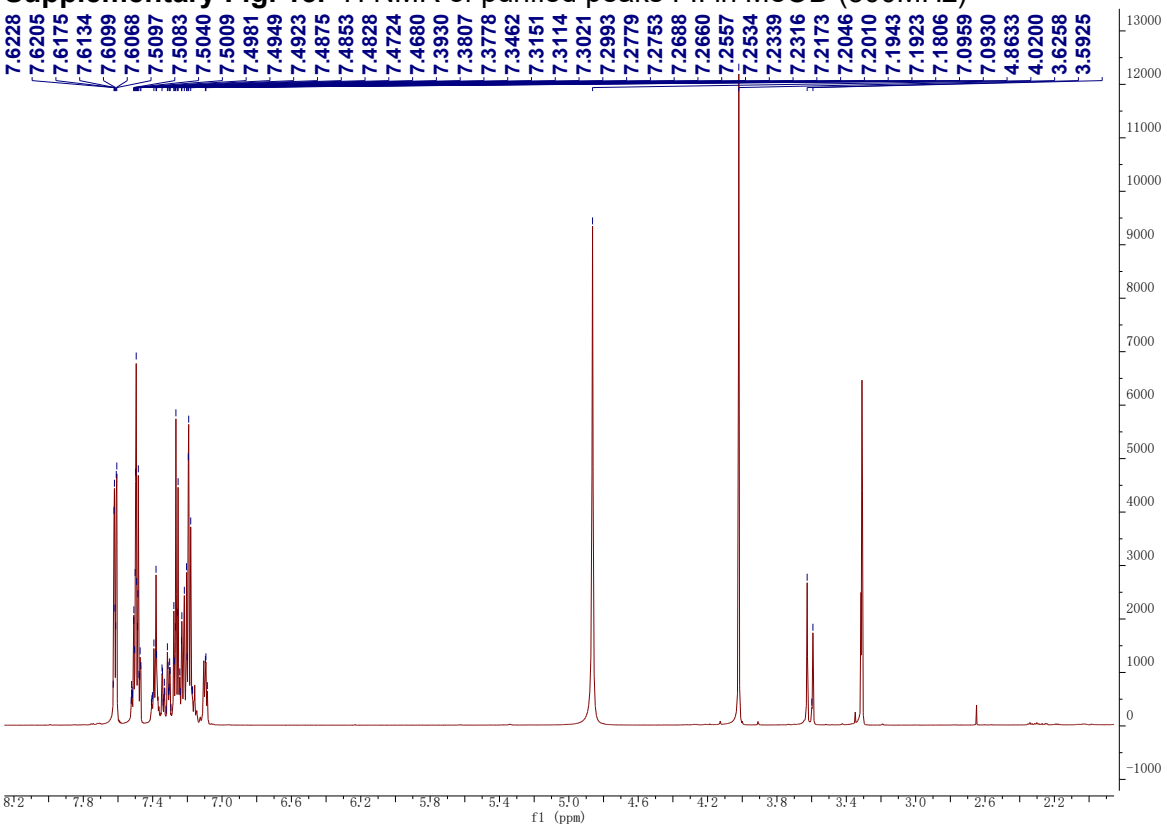

Supplementary Fig. 14. ^{1}H NMR of purified peak III in MeOD (500MHz)

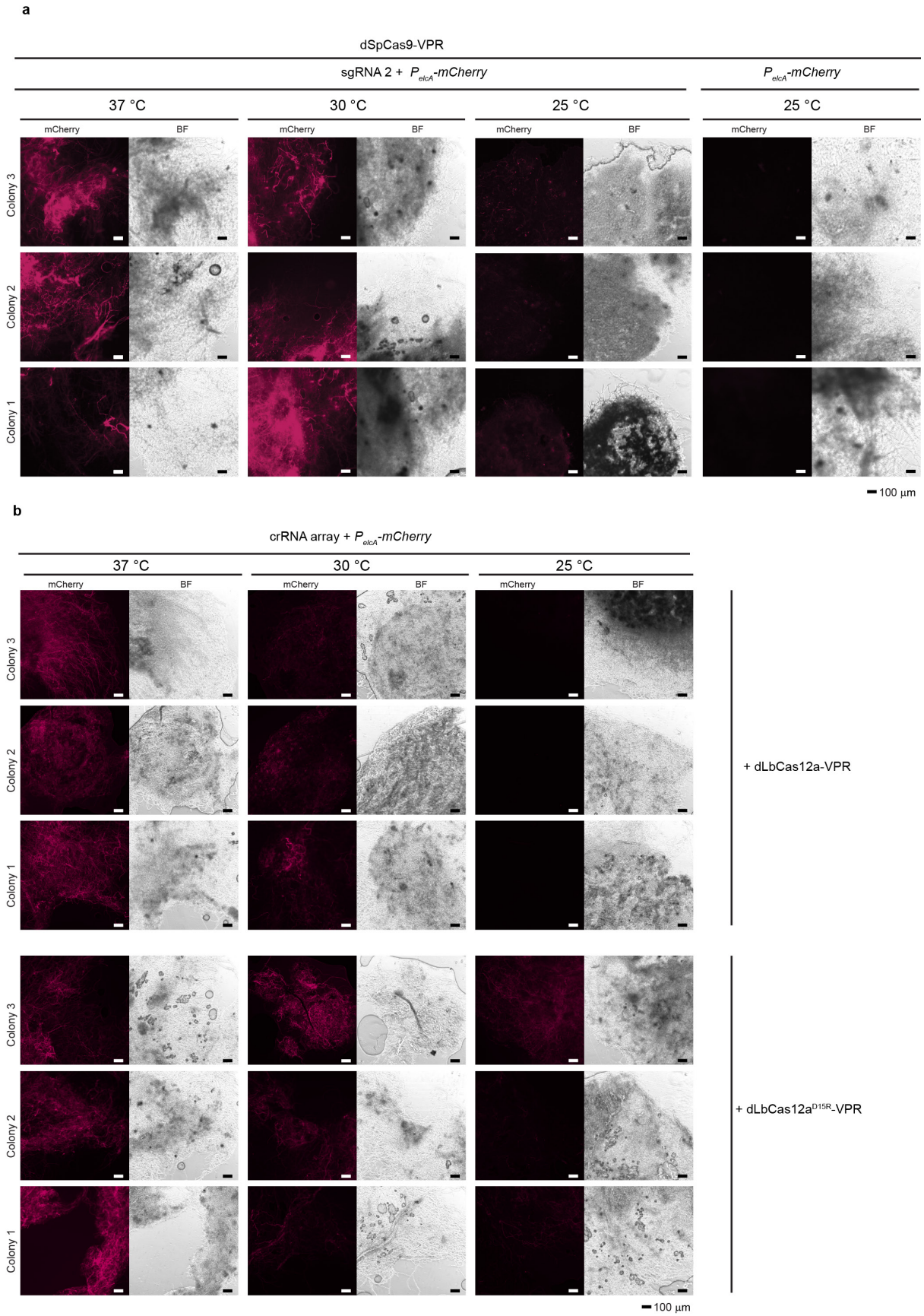

Supplementary Fig. 15 CRISPR-mediated activation of P_{elcA}-*mcherry* fluorescent reporter is limited at low temperatures . **a**. The activation observed in mycelia by CRISPR/dspCas9-VPR

846 at 37 °C is similar to that observed at 30 °C but lower at 25 °C in mycelia at a stage of
847 equivalent growth to that observed in the other temperature conditions. Fluorescence at 25 °C
848 was still distinguishable from the no sgRNA control. **b**. CRISPR/dLbCas12a-mediated
849 activation was observed for mycelia grown at 37 °C and 30 °C but not observed at 25 °C. The
850 variant dLbCas12a^{D156R}-VPR presents observable fluorescence signal at 25 °C unlike the
851 original system. In all cases, the spores for each sample were collected from three individual
852 colonies and grown in liquid stationary culture overnight in the case of 37 °C, and 30 °C and
853 two days for the samples at 25°C. The photos represent the mCherry channel and bright-field
854 (BF). Scale bar 100 μm.

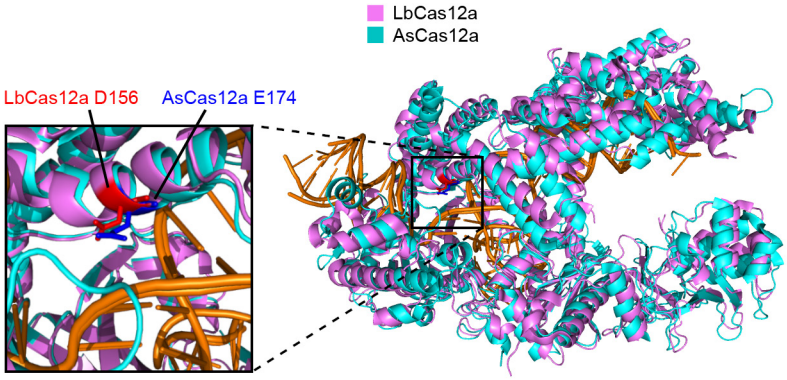

855

856 **Supplementary Fig. 16** Protein alignment visualised in Pymol of LbCas12a (pink) and
857 AsCas12a (light blue) crystal structures[2,3] indicates that residue D156 from LbCas12a (Red)
858 is an equivalent residue to E174 from AsCas12a (blue).

859

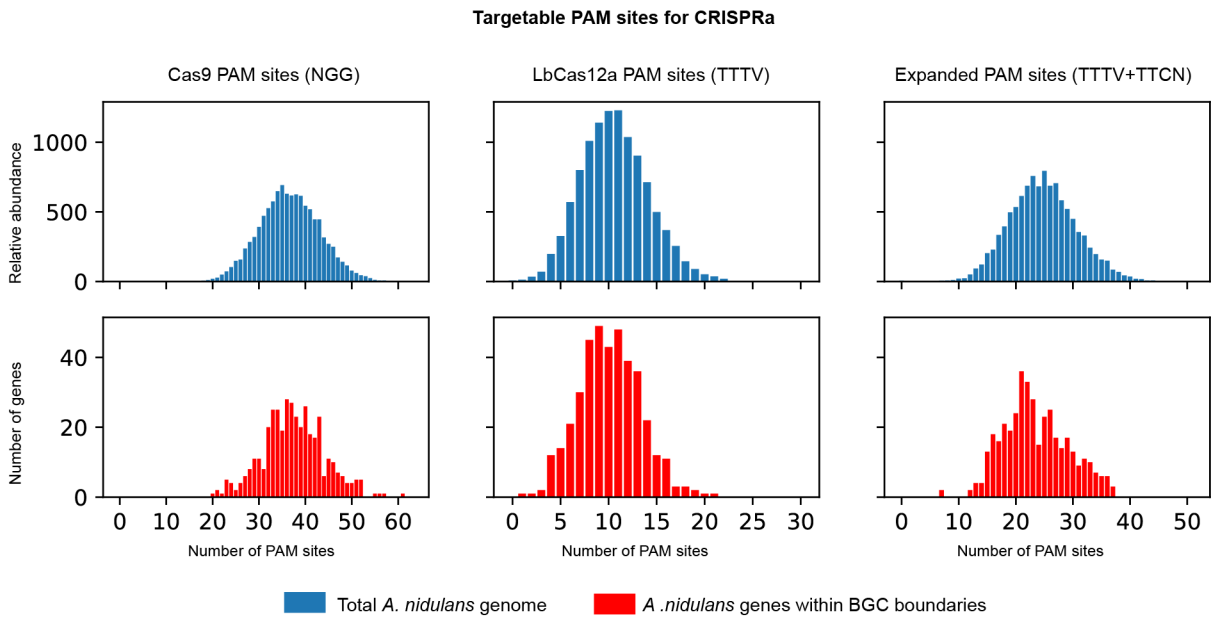

Supplementary Fig. 17 . Amount of PAM sites identified in the targetable window of *A. nidulans* genes (blue) and genes located in BGCs (red). Targetable window was defined as 400bp upstream of the start of the gene (TSS if available, otherwise -100bp of the start codon) or shorter if intergenic distance is less than 400bp. Even though LbCas12a has fewer targeting sites compared to Cas9, the median is 10 PAM sites per gene. In cases with limiting number of PAM sites, the use of the non-canonical site TTCN with the dLbCas12a^{D156R}-VPR variant could be explored, at the cost of losing efficiency for the canonical site, based on our observations at 37 °C (see Fig 4).

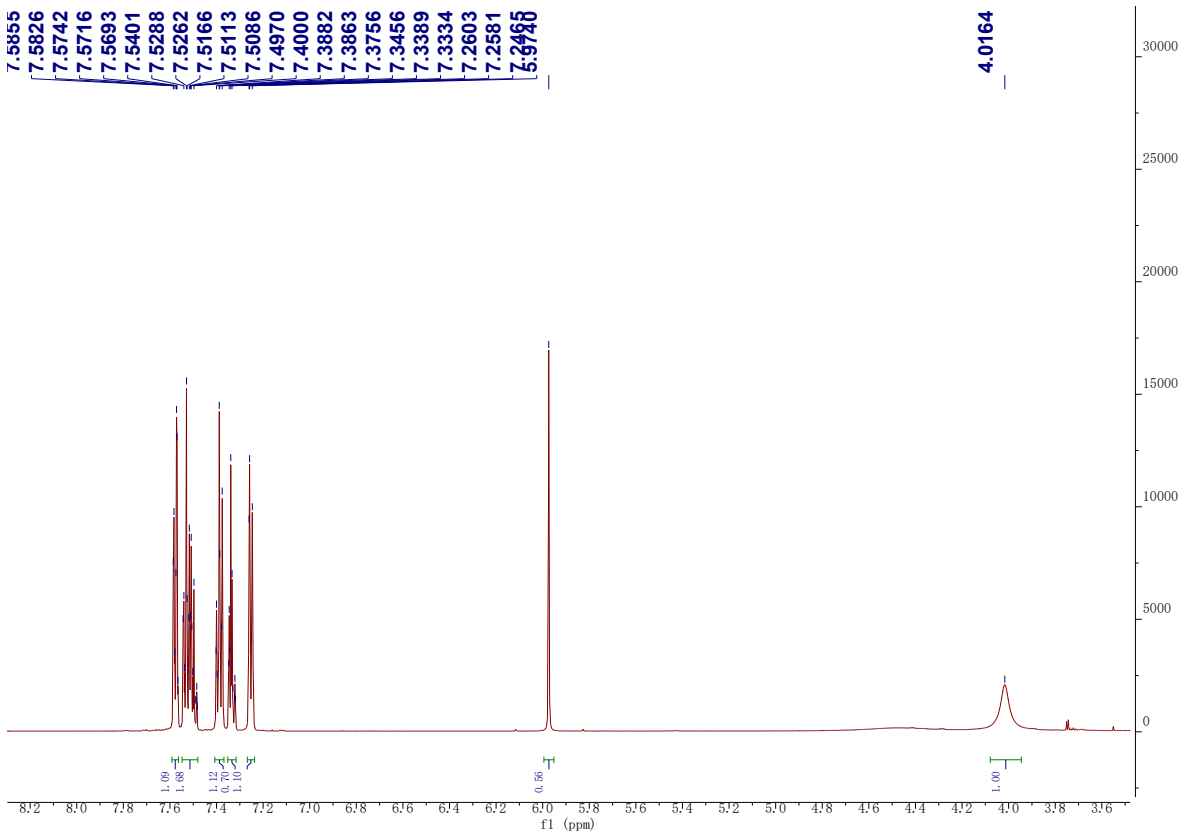

Supplementary Fig. 18 ^{1}H NMR spectrum (600 MHz) of microperfuranone in $CDCl_3$-*d*.

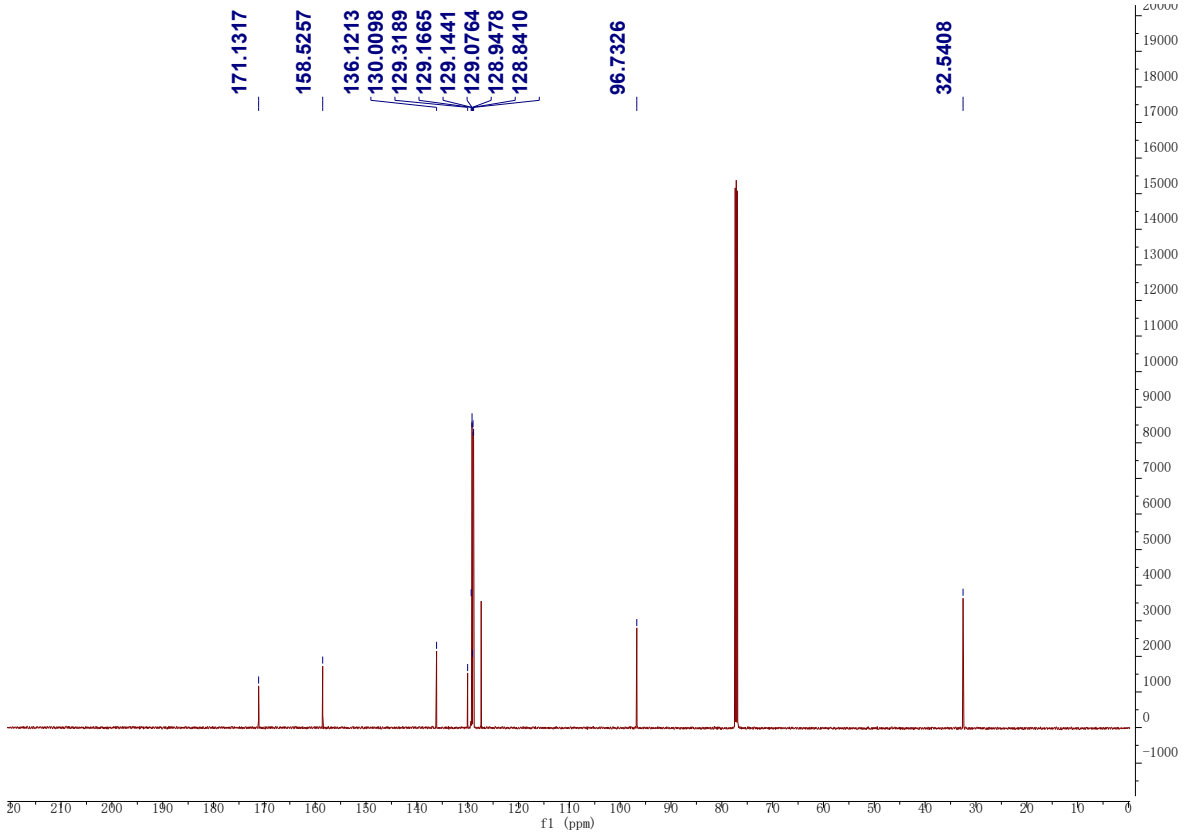

Supplementary Fig.19 ^{13}C NMR spectrum (150 MHz) of microperfuranone in $CDCl_3$-*d*.

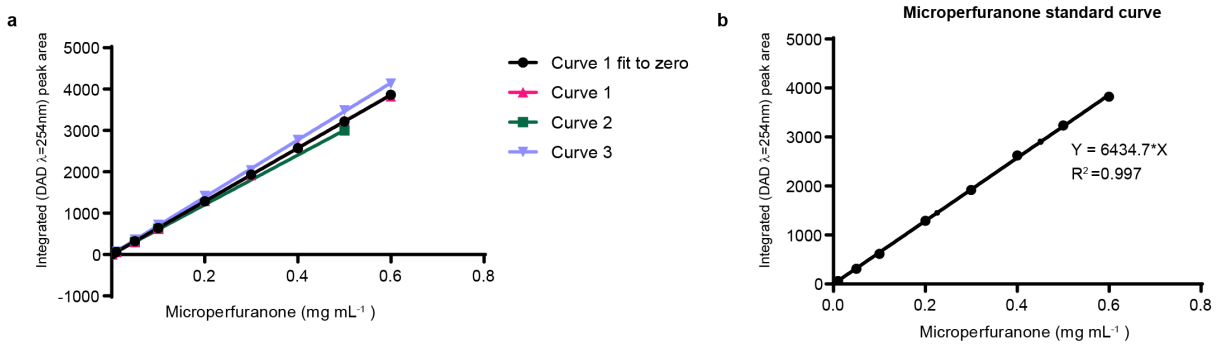

877
878
879 **Supplementary Fig. 20**. Calibration curve used for microperfuranone quantification. **a.**
880 Different calibration curves reproduce linearity but reflect the error from weighting
881 microperfuranone with the analytical balance. Individual values indicated as points. **b.** Curve
882 1 fit to zero was chosen as representative for quantification, points are the mean of three LC-
883 DAD-MS injection technical replicates per point, SD is represented.
884

Supplementary Tables

Supplementary Table 1. Predicted spectra of dehydromicroperfuranone based on CFM-ID[4] is compared to LC-MS/MS (MS^2) spectra of m/z 265 at different fragmentation events.

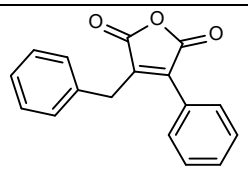

Dehydromicroperfuranone

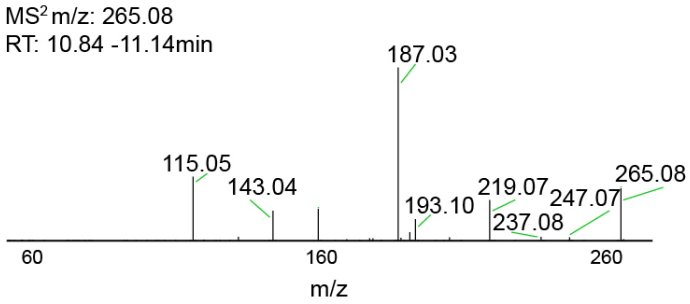

Theoretical fragment m/z by CFM-ID[4]	Observed m/z	Error (ppm)	Mass difference (Da)	Proposed structure by CFM-ID
265.0859207	265.079	-26.1080659	0.0069207	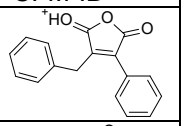
247.075356	247.0688	-26.53511896	0.006556	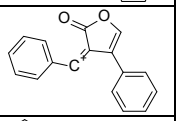
237.0910061	237.0847	-26.598511	0.0063061	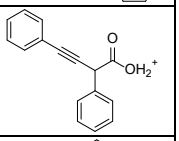
219.0804414	219.0745	-27.12045446	0.0059414	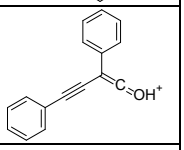
193.1011768	193.0959	-27.32735392	0.0052768	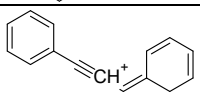
187.0389705	187.0337	-28.17941366	0.0052705	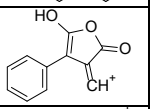
143.0491413	143.0451	-28.25192894	0.0040413	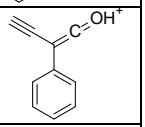
115.0542266	115.0509	-28.91415886	0.0033266	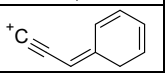

Supplementary Table 2. ^{1}H and ^{13}C NMR data for dehydromicroperfuranone (**2**) purified as peaks I-II and peak III showing identical chemical shifts in chloroform-*d* (Supplementary Fig. 9–12). a: overlapping peaks, or tentatively assigned based on prediction. The previously reported NMR chemical shifts for **2**[5] are shown in the table for comparison.

	2 in Chloroform-*d* Ref. [5]		**Peaks I-II** in Chloroform-*d* This work		**Peak III** in Chloroform-*d* This work	
Carbon No.	^{13}C NMR	^{1}H NMR	^{13}C NMR	^{1}H NMR	^{13}C NMR	^{1}H NMR
2	165.8 (s)	-	166.0 (s)	-	165.9 (s)	-
3	141.0 (s)	-	141.2 (s)	-	141.3 (s)	-
4	135.5 (s)	-	135.5 (s)		135.6 (s)	-
5	164.8 (s)		165.0 (d)	-	165.0 (s)	-
6	127.1 (s)	-	127.2 (s)	-	127.3 (s)	-
7	128.4 (d)	7.15 (5H, br s)[a]	129.23 (d)	7.21 (m)[a]	129.3 (d)[a]	7.21 (m)[a]
8	129.0 (d)	7.44 (5H, br s)[a]	129.17 (d)	7.63 (m)[a]	129.2 (d)[a]	7.63 (m)[a]
9	130.2 (d)	7.44 (5H, br s)[a]	131.3 (d)	7.55 (m)[a]	131.4 (s)	7.55 (m)
10	129.0 (d)	7.44 (5H, br s)[a]	129.17 (d)	7.63 (m)[a]	129.2 (d)[a]	7.63 (m)[a]
11	128.4 (d)	7.15 (5H, br s)[a]	129.23 (d)	7.21 (m)[a]	129.3 (d)[a]	7.21 (m)[a]
12	30.4 (t)	3.93 (2H, s)	30.6 (s)	4.03 (2H, s)	30.6 (s)	4.05 (2H, s)
13	140.6 (s)	-	140.8 (s)	-	140.8 (s)	-
14	129.3 (d)	7.15 (5H, br s)[a]	128.6 (d)	7.34 (m)[a]	128.6 (d)	7.34 (m)
15	129.0 (d)	7.44 (5H, br s)[a]	129.5 (d)	7.53 (m)[a]	129.5 (d)[a]	7.53 (m)[a]
16	127.3 (s)	7.15 (5H, br s)[a]	127.5 (d)	7.29 (m)[a]	127.5 (s)	7.28 (m)
17	129.0 (d)	7.44 (5H, br s)[a]	129.5 (d)	7.53 (m)[a]	129.5 (d)[a]	7.53 (m)[a]
18	129.3 (d)	7.15 (5H, br s)[a]	128.6 (d)	7.34 (m)[a]	128.6 (d)	7.34 (m)

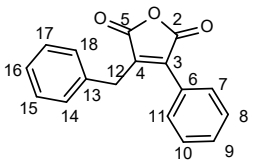

Dehydromicroperfuranone (2)

Supplementary Table 3. ^{1}H and ^{13}C NMR data for microperfuranone (**1**) in chloroform-*d* (supplementary Fig. 18–19). a: overlapping peaks, or tentatively assigned based on prediction. The previously reported NMR chemical shifts for **1**[6,7] are shown in the table for comparison.

Carbon No.	**1** in acetone-d_6 Ref.[6]		**1** in Chloroform-*d* Ref.[7]		**1** in Chloroform-*d* This work	
	^{13}C NMR	^{1}H NMR	^{13}C NMR	^{1}H NMR	^{13}C NMR	^{1}H NMR
2	170.9 (s)	-	171.6 (s)		171.1 (s)	-
3	130.8 (s)	-	129.7 (s)		130.0 (s)	-
4	159.6 (s)	-	158.9 (s)		158.5 (s)	
5	97.7 (d)	5.98 (br s)	97.2 (d)	5.89 (br s)	96.7 (d)	5.97 (br s)
5-OH	-	6.90 (br s)		N/A	-	N/A
6	130.2 (s)	-	129.1 (s)		129.1 (s)	-
7	129.9 (d)	7.54 (br d, 6.7)	129.0 (s)	N/A	129.2 (d)	7.57 (m)[a]
8	129.3 (d)	7.46 (m)	128.6 (d)	N/A	128.8 (d)	7.50 (m)[a]
9	129.6 (d)	7.43 (m)	128.9 (d)	N/A	128.9 (d)	7.52 (m)[a]
10	129.3 (d)	7.46 (m)	128.6 (d)	N/A	128.8 (d)	7.50 (m)[a]
11	129.9 (d)	7.54 (br d, 6.7)	129.0 (s)	N/A	129.2 (d)	7.57 (m)[a]
12	32.9 (t)	3.97 (2H, br s)	32.3 (s)	3.91 (2H, br s)	32.3 (s)	3.97 (2H, br s)
13	137.5 (s)	-	136.0 (s)		136.1 (s)	-
14	129.6 (d)	7.30 (m)	128.8 (d)	N/A	128.9 (d)	7.26 (m)[a]
15	129.7 (d)	7.26 (m)	128.9 (d)	N/A	129.1 (d)	7.34 (m)[a]
16	127.7 (d)	7.22 (m)	127.1 (d)	N/A	127.3 (d)	7.33 (m)[a]
17	129.7 (d)	7.26 (m)	128.9 (d)	N/A	129.1 (d)	7.34 (m)[a]
18	129.6 (d)	7.30 (m)	128.8 (d)		128.9 (d)	7.26 (m)[a]

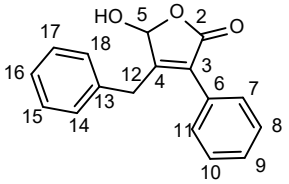

Microperfuranone (1)

904

905 Additional Supplementary Tables 4-9 are found as tabs an Excel file:

906 Supplementary Table 4 : Strains used in this study

907 Supplementary Table 5 : Plasmids used in this study

908 Supplementary Table 6 : Protospacers targeted

909 Supplementary Table 7 : Oligonucleotides used to create crRNA/sgRNA

910 Supplementary Table 8 : Oligonucleotides

911 Supplementary Table 9 : Statistical Analysis

912

913 **Supplementary note 1 : Sequence of crRNA expression cassettes cloning sites**

914 **> Cloning site of *P_{gpda}* *LbCas12a* crRNA cassette**

915 **(…)ATCTTCCCATCCAAGAACCTTTAATC**AAGCTTATCGATACCGTCGACCTCGACTCTA
916 GAGGATCG***AATTTCTACTAAGTGTAGAT***GGAGACGAGAATTCCGTCTCC***AATTTCTACT***
917 ***AAGTGTAGAT***ATCTTCGAGGGGGGGCCCGGTACCGCCCCGTCCGGTCCTGCCCGTCA
918 CCGA**GATCCACTTAACGTTACTGAAATCAT(…)**

919 *A. nidulans P_{gpdA}* TSS(bold underlined) and *gpdA* 5'UTR (bold green underlined). LbCas12a

920 scaffold (blue italics). BsmbI sites (underlined) .EcoRI site (red). **TrpC Terminator (black**

921 **bold)**

922

923 **> Cloning site of *P_{U3}* *SpCas9* sgRNA cassette**

924 *TTAATTAA***(...)CAAGTCAGAACATTTTGCTAACAGC**AGAGACGGGCGCCGCTACAGGGC
925 GCGTCCCATTCGCCATTCAGGCTGCGCAACTGTTGGGAAGGGCGATCGGTGCGGGCC
926 TCTTCGCTATTACGCCAGCTGGCGAAAGGGGGATGTGCTGCAAGGCGCGTCTCC*GTTT*
927 *TAGAGCTAGAAATAGCAAGTTAAAATAAGGCTAGTCCGTTATCAACTTGAAAAAGTGGC*
928 *ACCGAGTCGGTGC***TTTTTTTT**CC*GCGGCCGC*CTGCAGGTCGACCATA(…)

929 PacI site (orange italics underlined) ***A. fumigatus U3* promoter (bold green)**. *SpCas9*

930 *sgRNA scaffold (blue italics).* BsmbI sites (underlined) .LacZ fragment (red). Poly T

931 terminator (bold) . NotI site (purple italics underlined)

932

933 **References**

934 1. Sibthorp, C. *et al.* Transcriptome analysis of the filamentous fungus *Aspergillus*
935 *nidulans* directed to the global identification of promoters. *BMC Genomics* **14,** 847
936 (2013).

937 2. Yamano, T. *et al.* Crystal Structure of Cpf1 in Complex with Guide RNA and Target
938 DNA. *Cell* **165,** 949–962 (2016).

939 3. Yamano, T. *et al.* Structural Basis for the Canonical and Non-canonical PAM

940 Recognition by CRISPR-Cpf1. *Mol. Cell* **67,** 633–645.e3 (2017).

941 4. Allen, F., Pon, A., Wilson, M., Greiner, R. & Wishart, D. CFM-ID: A web server for
942 annotation, spectrum prediction and metabolite identification from tandem mass
943 spectra. *Nucleic Acids Res.* **42,** (2014).

944 5. Hamasaki, T., Nakajima, H., Yokota, T. & Kimura, Y. A New Metabolite, 3-Carboxy-
945 2,4-diphenyl-but-2-enoic Anhydride, Produced by *Aspergillus nidulans*. *Agric. Biol.*
946 *Chem.* **47,** 891–892 (1983)

947 6. Fujimoto, H., Asai, T., Kim, Y. P. & Ishibashi, M. Nine constituents including six
948 xanthone-related compounds isolated from two ascomycetes, *Gelasinospora santi-*
949 *florii* and *Emericella quadrilineata*, found in a screening study focused on
950 immunomodulatory activity. *Chem. Pharm. Bull.* **54,** 550–553 (2006).

951 7. Yeh, H. H. *et al.* Molecular genetic analysis reveals that a nonribosomal peptide
952 synthetase-like (NRPS-like) gene in *Aspergillus nidulans* is responsible for
953 microperfuranone biosynthesis. *Appl. Microbiol. Biotechnol.* **96,** 739–748 (2012).

954 .

955

956